Applied Energy 393 (2025) 126103

Contents lists available at ScienceDirect

Applied Energy

journal homepage: www.elsevier.com/locate/apenergy

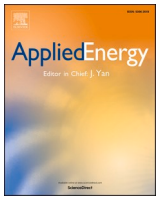

Simulation and performance optimization of a novel hybrid CCHP system based on the prime movers of internal combustion engine and Stirling engine

Mohammad Sheykhi [a,*], Mahmood Mehregan [a,*], Saeed Ghorbani [b], Amin Emamian [c], Mohammad Hassan Kayhani [a], Amin Amiri Delouei [c], Shahabodin Kharazmi [d], Mohammad Kazem Sheykhian [a], Shunmin Zhu [e,*]

[a] Faculty of Mechanical Engineering, Shahrood University of Technology, Shahrood, P.O.B, 3619995161, Iran
[b] Department of Mechanical Engineering, Faculty of Advanced Technologies, Quchan University of Technology, Quchan, Iran
[c] Department of Mechanical Engineering, University of Bojnord, Bojnord, Iran
[d] Faculty of Mechanical Engineering, Semnan University, Semnan, Iran
[e] Department of Engineering, Durham University, Durham DH1 3LE, UK

HIGHLIGHTS

- Proposes a novel CCHP system arrangement including an ICE and an SE in parallel.
- The current arrangement has an appropriate technical performance at high SE speeds.
- The optimal range of the system conditions was identified technically and economically.
- The CCHP system shortens the SPP by 1.6 years compared to an ICE-only system.

ARTICLE INFO

Keywords:
CCHP
Internal combustion engine
Stirling engine
Porosity
Spark timing
Investment payback period

ABSTRACT

Combined cooling, heating, and power systems (CCHP) could increase the efficiency of conventional energy supply systems and mitigate carbon emissions. In this paper, a novel arrangement of a combined cooling, heating, and power (CCHP) system is presented with prime movers of internal combustion and Stirling engines, which are numerically simulated by Range-Kutta method and optimized with the genetic algorithm technique. The influence of some key parameters such as Stirling engine speed, phase angle, length and porosity of Stirling engine's regenerator, and also speed and spark timing of the internal combustion engine, on the capacity, efficiency, primary energy saving and the investment payback period of the CCHP system has been discussed. The results illustrated that using the CCHP system with hybrid prime movers, due to the appropriate efficiency of the combustion engine, allows the Stirling engine to be started at high speeds. In this condition, the overall efficiency of the hybrid system is increased by 12 % compared to using the CCHP system with only the Stirling engine. Additionally, the payback period of the CCHP system with combined prime movers at 3500 rpm for the two engines is approximately 4.4 years, which is about 1.6 years shorter than the payback period of the CCHP system based solely on the internal combustion engine. This work provides valuable insights into the design and optimization of hybrid CCHP systems with two different combustion-based prime movers.

1. Introduction

Combined cooling, heating, and power systems (CCHP) have been proposed to increase the efficiency of conventional energy supply systems and mitigate the emission impact of harmful environmental pollutants such as CO, CO_2, and NOx [1]. These systems employ the mechanical power generated by a prime mover to supply electricity and utilize its waste heat for providing cooling and heating with the help of an absorption chiller and a heat recovery system (heat exchanger) [2]. In

* Corresponding authors.
E-mail addresses: Mohammad.Sheykhi20@gmail.com (M. Sheykhi), mehregan@shahroodut.ac.ir (M. Mehregan), shunminzhu@durham.ac.uk (S. Zhu).

https://doi.org/10.1016/j.apenergy.2025.126103
Received 9 February 2025; Received in revised form 8 May 2025; Accepted 10 May 2025
Available online 19 May 2025

Nomenclature

Abbreviations

ACS	Annual Cost Saving
CCHP	Combined Cooling, Heating, and Power
CHP	Combined Heat and Power
CSP	Concentrated Solar Power
COP	Coefficient of Performance
DPP	Discounted Payback Period
ICE	Internal Combustion Engine
IPP	Investment Payback Period
LHV	Lower Heating Value
LPG	Liquefied Petroleum Gas
NTU	Number of Transfer Units
SE	Stirling Engine
SPP	Simple Payback Period

Symbols

AF	mass ratio of air to fuel, (−)
A_{wg}	wetted surface of the regenerator (cm^2)
C_p	specific heat at constant pressure (J/kg.K)
C_v	specific heat at constant volume (J/kg.K)
D_{hr}	hydraulic diameter (cm)
d_m	diameter of the wires, (cm)
f	frictional coefficient, (−)
fr	frequency of engine, (HZ)
G	gas mass flow per unit area, (kg/m^2.s)
h	Convective heat transfer coefficient, (W/m^2.K)
L_{reg}	regenerator length, (cm)
M	mass of the working gas, (gr)
M	annual maintenance cost, £
m_f	mass flow rate of fuel, (gr/h)
N_r	internal combustion engine speed, (rpm)
n_{cyl}	number of cylinders, (−)
n_r	Stirling engine speed, (rpm)
P	power, (kW)
p	pressure, (MPa)
Pr	Prantel number, (−)
Q	heat transfer (J)
R	gas constant, (J/kg.K)
Re	Reynolds number (−)
s	piston stroke, (cm)
St	Staunton number, (−)
T	temperature, (K)
V	volume, (cm^3)
V_d	displacement volume, (cm^3)
W	work output (J)
x	fuel heat release function

Greek

α	phase angle, (deg)
η	efficiency (−)
μ	dynamic viscosity (kg/m.s)
ε	effectiveness, (−)
γ	specific heat ratio, (−)
φ	porosity coefficient, (−)
θ	crank angle, (deg)

Subscripts

c	compression chamber
comb	Combustion
e	expansion space
ex	exhaust
f	fuel
h	heater
hr	hydraulic
k	cooler
r	regenerator
swc	compression
swe	expansion
wg	wetted

this way, the energy efficiency increases and the economic costs decrease [3]. Nonetheless, in some cases, the initial costs (implementation costs) of these systems might be higher than conventional energy supply systems. Therefore, each proposed CCHP system must be meticulously appraised from an economic standpoint. The annual profit of the proposed system compared to conventional systems should be calculated, and an investment payback period (IPP) should be gauged [4]. This economic analysis is more valid when annual inflation is included [5]. One of the principal components of CCHP systems that has a significant impact on energy efficiency, fuel consumption, harmful emissions as well as economic performance is the prime mover [6]. The appropriate selection of the prime mover should usually be made according to the capacity and type of system use, weather conditions and energy prices [7].

One of the prime movers of CCHP systems is internal combustion engine (ICE) [8]. Whereby the chemical energy of the fuel is converted into mechanical and heat energy through combustion inside the cylinder chamber [9].

Among the advantages of ICEs, we can mention high power output relative to the engine volume and suitable thermal efficiency at different engine speeds [9]. Nonetheless, ICEs have some disadvantages, such as restrictions on the use of certain fossil fuels, relatively high pollution emissions, and significant noise [10,11].

Another prime mover of CCHP systems is the Stirling engine (SE) [12]. SEs are a type of external combustion engine that can produce power based on the compression and expansion of a working gas, such as helium or hydrogen at different temperatures [13]. The initial application of these engines was to pump water. Other uses include its implementation in concentrated solar power (CSP) [14], combined heat and power (CHP) [15] and submarine propulsion [16]. The advantages of SEs include low noise, low emission, and the ability to run on a variety of fuels, such as fossil fuels, biomass, nuclear, and solar energy [17,18]. However, in SEs, a considerable amount of time is needed for heat to be transferred from an external source to the engine, and the reactivity of these engines is weaker than ICEs at different engine speeds and loads [19]. Additionally, at high speeds, these engines usually do not have good thermal efficiency [20].

So far, some research have been focused on the modeling and optimization of CHP and CCHP systems based on ICEs and SEs. Ehyaei et al. [21] presented a CCHP system based on an ICE to supply the energy demand for a building in Iran, taking into account the cost of air pollutant taxes, namely, carbon dioxide, nitrogen monoxide, and carbon monoxide. They indicated that the average cost of generating electricity for the system would be 0.05 $/kWh. In a study by Zheng et al. [22], a dynamic simulation of a CHP unit with an ICE was presented, and the start-stop interval of the system was analyzed. The results of the model illustrated that the interval of start-stop was more than 0.5 h for the CHP-ICE system to achieve the maximum amount of fuel consumption savings. In the work of Wei et al. [23], the potential of using a 12-cylinder gas-burning engine as the primary driver of the combined system was investigated. The engine performance was analyzed, and the parameters of spark timing were checked. The results showed that the ratio

of heat to power can be changed in the range of 1 to 1.6. Muccillo and Gimelli [24] experimentally and numerically modeled a small-scale CHP system based on a liquefied petroleum gas (LPG) engine. They showed that the desired system is suitable for energy supply in residential buildings, hospitals, hotels, and sports centers. Aghaei Meybodi and Behnia [7] investigated the CHP systems based on gas and diesel combustion engines, considering the carbon tax. The results showed that the carbon tax has a great impact on prolonging the investment return period, and the CHP systems with diesel engines are not very economical.

Arbabi et al. [25] reported that a cogeneration system with gas engine and a capacity of 85 kW can have an energy efficiency of 81 % and a IPP of 7.5 years. Balakheli et al. [26] studied different arrangements of cogeneration systems based on ICE. In their study, the effect of engine speed was investigated. The results indicated that if a compression chiller is used to provide cooling, the system will perform well from an environmental point of view and will emit less carbon dioxide than other arrangements, but because the fuel consumption costs are high, it is not suitable from economic perspective. Sheykhi et al. [27] studied a CCHP system with a gas engine and analyzed the impact of engine compression ratio and speed, on system specific fuel consumption. In another study presented by Sheykhi and Mehregan [28], a CCHP system with a gas engine was simulated from economic and technical perspectives at different engine speeds, and the effects of ignition timing on internal return rate (IRR) and net present value were investigated. The results indicated that at high engine speeds and optimal ignition timing, the IRR of the CCHP system reaches 24 % after 8 years.

The work of Kong et al. [29] can be mentioned among the first researches carried out in the field of CCHP systems with a SE as the prime mover. In this research, a general evaluation of the implementation of a trigeneration system based on the SE was done according to the price of natural gas in Shanghai and Beijing. In this study, the system IPP was calculated in about 2 to 3.5 years according to the cost of natural gas fuel. Also, 33 % energy savings were reported for this system compared to conventional systems. Karami and Sayyaadi [30] showed that a CCHP system based on the SE in Bandar Abbas, Iran, cannot be economically justified due to the low tariffs for purchasing electricity and high tariffs for purchasing natural gas. On the other hand, they report that the implementation of this system in Yazd city in Iran is economically justified according to the city's energy tariffs, and the IPP for it is about 4 years. Skorek et al. [31] showed that a small-scale SE cogeneration system has an electrical efficiency in the range of 20–30 %. Also, in this system the carbon dioxide emissions were reduced in the range of 10 to 64 %.

Using a non-ideal adiabatic model, Chahartaghi and Sheykhi [32] illustrated that the use of a trigeneration system with a SE and working gas of hydrogen has better performance than helium. In another research conducted by Sheykhi et al. [33], it was showed that a small-sized power and heat cogeneration system at low SE speeds can have good efficiency and performance. Also, this system was able to reduce the amount of carbon dioxide emission tax by about $ 900 per year compared to conventional systems. In the experimental work done by Hidalgo et al. [34], a CHP system with a solar SE was developed. In this study, the cogeneration system supplied about 75 % of the energy needed by a building for a typical family, and the reduction in carbon dioxide emissions from the system was reported in the range of 36 %. In a study, a technical and economic modeling and optimization was done by Sheykhi and Mehregan [35], and under optimal conditions for CCHP system with a SE, special fuel consumption and IPP were evaluated.

It is known that ICEs are the most common prime movers of cogeneration and trigeneration systems. However, due to limitations such as: the utilization of specific fossil fuels, and the environmental and noise emissions, it is not suitable for the ICE to bear the full load of the cogeneration system. Considering the advantages of SEs, such as high thermal efficiency, especially at low speeds, low noise and emissions, and the ability to use a variety of energy sources, it is better if half of the load of the system is on the SE. On the other hand, SEs do not have good thermal efficiency at high speeds, and it is better to use ICEs that have good thermal efficiency at all speeds in combination with SEs to achieve high capacities in combined systems. In this way, the limited studies that have been carried out for CHP and CCHP systems with these two prime movers are presented.

One of the first studies in the field of CHP systems based on ICE and SE in a hybrid manner is the work of Li et al. [36]. They presented a laboratory model of a power and heat production system. In their work, the thermal energy of exhaust gases of a gasoline ICE was used as the heat source of a beta-type SE. Results showed that the waste heat of an ICE can be a valuable heat source for the SE, and by using two engines in a combined manner, the efficiency of the CHP system increases. In another study, Sheykhi et al. [37] developed the work of Li et al. [36], numerically and discussed it from the environmental and economic issues at different engine speeds. In their work, the carbon dioxide was decreased by about 10 % compared to a conventional CHP system with an ICE, and the system reached profitability after 10 years. In another study, Jia and Paul [38] proposed a CCHP system with ICE and SE as prime movers. The modeling was done numerically, and the results illustrated that the overall efficiency of the system is about 62 %. Also, they analyzed engine speeds on profitability of the system.

SEs usually do not have good thermal efficiency at high speeds, and using these engines at high speeds as the prime mover of CCHP systems can reduce energy efficiency and increase fuel consumption of this systems, and it is usually appropriate to use these engines at lower capacities. On the other hand, due to the high capital cost of ICEs, it is not economically appropriate to operate a CCHP system based on an ICE at low speeds, and using these systems at higher capacities is more appropriate. Thus, using these two prime movers as a hybrid in optimal operating conditions can improve the technical and economic performance of CCHP systems. It is noteworthy that optimizing other geometric and functional parameters of these two engines, including spark timing, heat regenerator characteristics, and phase angle, can further contribute to the commercialization of these systems in construction users.

So in this study, a comprehensive simulation of the technical and economic performances of a CCHP system based on the gas-burning ICE (EF7) and the alpha-type Stirling engine (Ford-Phillips) has been conducted in a parallel hybrid form, and for the first time the impacts of some parameters of the prime movers including spark timing, ICE speed, regenerator length, regenerator porosity, SE phase angle and speed on the technical performance of the CCHP system, such as the overall efficiency and primary energy savings are discussed. Furthermore, economic performance indexes, including the IPP are determined by considering different economic inflations. It is noteworthy that the changes in these parameters can have opposite influences on the technical and economic performance of the system. So, it is recommended to determine the appropriate values based on the type of use and the project's goals. In addition to these, in this work, with the help of genetic algorithm and LINMAP decision-making method, the most optimal working conditions of the CCHP system from the technical and economic points of view have been identified. The innovations and highlights of the current work are summarized below:

- Proposing a CCHP system based on the novel arrangement of the prime movers including a gas ICE and an alpha SE in parallel.
- Simulating the impacts of the prime movers' characteristics, on the technical and economic performances of the CCHP system.
- Finding the optimal range of operational conditions of the CCHP system from technical and economic perspectives.

2. Simulation

2.1. CCHP system design

The schematic design of the proposed CCHP system with prime movers of the EF7 gas ICE and the Ford-Phillips SE is presented in Fig. 1. The heat source for the SE is provided by burning natural gas. As shown in Fig. 1, the cooling of the building is provided by two single-effect absorption chillers utilizing the waste heat of exhaust gases of the gas engine and part of the heat rejected from the Ford-Phillips Stirling engine cooler. Also, the heating of the building is achieved using two heat exchangers (heat recovery system) that harness the heat rejected by the gas engine cooling system and the Stirling engine cooler. Additionally, the output mechanical power of the two engines is directed to the power generators to produce electric power.

2.2. Combustion engine simulation

By applying the mass and energy conservation laws for the cylinder of an ICE (Fig. 2) at different rotation speed and considering heat and mass losses of the cylinder, the governing equations of this engine can be presented in a differential and dimensionless form [39].

Thus, the dimensionless differential equations of pressure, work, heat loss to the cylinder wall or heat loss to the cooling system as well as mass loss are presented in Eqs. (1) to (4), respectively [39].

$$\frac{d\tilde{p}}{d\theta} = -\gamma\frac{\tilde{p}}{\tilde{V}}\frac{d\tilde{V}}{d\theta} + \frac{(\gamma-1)}{\tilde{V}}\left[\frac{d\tilde{Q}}{d\theta} - \tilde{h}\left(1+\beta\tilde{V}\right)\left(\frac{\tilde{p}\tilde{V}}{\tilde{m}} - \tilde{T}_w\right)\right] - \frac{\gamma C_0\tilde{p}}{\omega} \tag{1}$$

$$\frac{d\tilde{W}}{d\theta} = \tilde{p}\frac{d\tilde{V}}{d\theta} \tag{2}$$

$$\frac{d\tilde{Q}_{loss}}{d\theta} = \tilde{h}\left(1+\beta\tilde{V}\right)\left(\frac{\tilde{p}\tilde{V}}{\tilde{m}} - \tilde{T}_w\right) \tag{3}$$

$$\frac{d\tilde{m}}{d\theta} = -C_0\frac{\tilde{m}}{\omega} \tag{4}$$

These four dimensionless linear equations form an ordinary differential equation system. Also, the dimensionless parameters mentioned in Table 1 are introduced [41]:

Subscript 1 denotes to the start of the compression stage. Also p, W, V_1, Q_{comb}, AF, LHV,m, η_v,η_{comb}, T_w, r_c, h, ω, and b are the pressure, net work, cylinder, heat from combustion, mass ratio of air to fuel, fuel heating value, fuel mass, volumetric and combustion efficiencies, cylinder wall temperature, compression ratio, heat transfer coefficients, engine speed and cylinder diameter.

In this study, the Wiebe function curve can be used to describe the combustion process. The fraction of the burned mass as a function of the crank angle grows from zero and exponentially tends to one, which indicates the end of combustion [42]. Thus, the Wiebe function is presented in Eq. (5) [43].

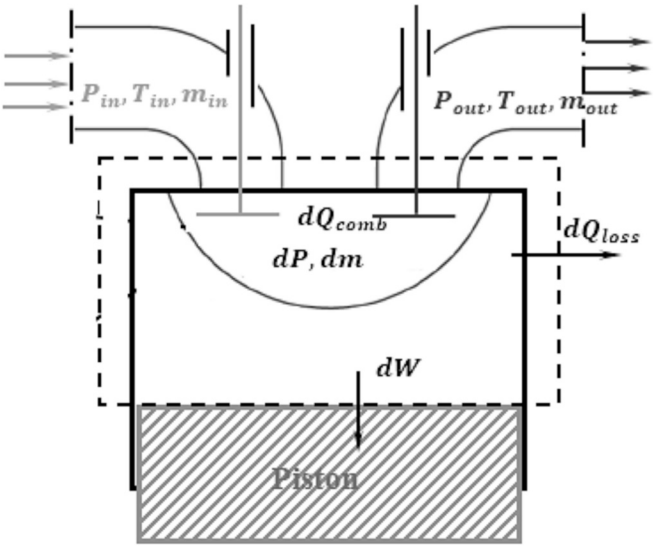

Fig. 2. ICE model [40].

Table 1
Dimensionless parameters of ICE model [41].

$\tilde{p} = \frac{p}{p_1}$	Dimensionless pressure
$\tilde{W} = \frac{W}{p_1 V_1}$	Dimensionless work
$\tilde{Q}_{loss} = \frac{Q_{loss}}{pV_1}$	Dimensionless heat to the cylinder wall
$\tilde{Q} = \frac{Q_{comb}}{p_1 V_1} = \frac{1}{1+AF}\frac{LHV}{RT_1}\eta_{comb} \bullet \eta_v$	Dimensionless heat from combustion
$\tilde{m} = \frac{m}{m_1}$	Dimensionless mass inside the cylinder
$\tilde{T}_w = \frac{T_w}{T_1}$	Dimensionless wall temperature
$\tilde{V} = \frac{V}{V_1} = \frac{\left[1+\frac{r_c-1}{2}(1-cos\theta)\right]}{r_c}$	Dimensionless volume
$\tilde{h} = \frac{4hT_1}{p_1\omega\beta b}$	Dimensionless heat transfer coefficient

$$x = 1 - exp\left[-a\left(\frac{\theta-\theta_s}{\theta_d}\right)^n\right] \tag{5}$$

where x is part of the released energy of the fuel, and θ, θ_s and θ_d are respectively the crank angle, ignition start angle, and combustion angle duration, Also, in Eq. (5), a and n are the Wiebe function constants and

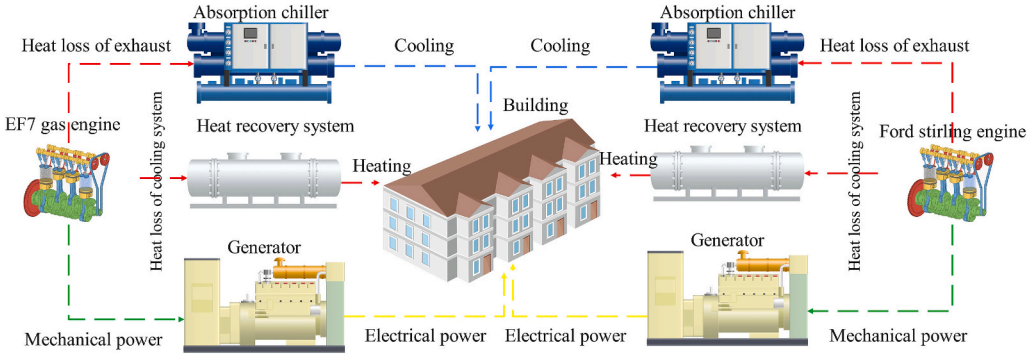

Fig. 1. CCHP system arrangement.

their values are equal to 5 and 3, respectively [43].

In Eq. (6), the brake power of the ICE (P_{ICE}) is given by [43].

$$P_{ICE} = P_{indi} - P_{loss} \tag{6}$$

$$P_{indi} = \frac{n_{cyl} W fr}{2} \tag{7}$$

$$P_{loss} = 10^5 \left[0.97 + 0.15 \left(\frac{Nr}{1000} \right) + 0.05 \left(\frac{Nr}{1000} \right)^2 \right] \frac{V_d n f r}{2} \tag{8}$$

Here, P_{indi}, P_{loss}, n_{cyl}, W, fr, Nr and V_d respectively are indicated power (theoretical), frictional power loss, number of cylinders, work output, engine frequency in rps, speed in rpm and volume displacement in the cylinder.

Also, the output torque of the ICE can be calculated according to Eq. (9) [40].

$$T_{ICE} = \frac{9550\, P_{ICE}}{Nr} \tag{9}$$

The heat loss rate to the cooling system of the ICE can be calculated according to Eq. (10) [40].

$$Q_{cool} = n Q_{loss} \frac{fr}{2} \tag{10}$$

The rate of waste heat from the ICE exhaust is presented by Eq. (11) [40].

$$Q_{ex} = Q_{comb} - Q_{cool} - P_{indi} \tag{11}$$

At the end, calculate the specific power fuel consumption according to Eq. (12).

$$PSFC = \frac{\dot{m}_f}{P_{ICE}} \tag{12}$$

It should be noted that the result of $\dot{m}_f LHV$ can be equal to the thermal energy released in the combustion process, or Q_{comb}.

2.3. Stirling engine simulation

One of the best choices for modeling the SEs is the adiabatic model. In fact, especially at high engine speed, the processes of expansion and compression in the SE are closer to the adiabatic state (without heat transfer). Therefore, by considering adiabatic assumptions instead of isothermal assumptions, the temperature in the compression and expansion chambers changes accordingly [44].

First, the main components of the SE are divided into independent sections for adiabatic analysis (Fig. 3). The main components of this engine include the expansion and compression chambers, cooler, heater, and regenerator.

For each part, taking into account the equations of conservation of energy and mass and the assumptions mentioned below, reversible adiabatic differential equations are derived [44].

- The processes of compression and expansion are adiabatic.
- Frictional pressure loss is not considered.
- Gas leakage in different components is ignored.
- The working gas of engine is ideal.
- The temperature of the working gas in the cooler and heater is assumed to be equal to the temperature of their walls.
- The temperature of the working gas is assumed to be constant at different points of the cooler and heater.
- There is no irreversible heat transfer in the regenerator.

The pressure equation can be expressed by following the ideal gas equation according to Eq. (13) [44]:

$$p = \frac{MR}{\frac{V_c}{T_c} + \frac{V_k}{T_k} + \frac{V_r}{T_r} + \frac{V_h}{T_h} + \frac{V_e}{T_e}} \tag{13}$$

Here, p is the pressure inside the engine, M, R and V represent the mass of the working gas, the gas constant and the volume of each element, respectively. Also, subscripts c, r, k, h, and e are respectively the specifications of compression chamber, regenerator, cooler, heater, and expansion chamber.

The differential form of the pressure equation is obtained as Eq. (14) [44]:

$$dp = \frac{-\gamma p \left(\frac{dV_c}{T_{ck}} + \frac{dV_e}{T_{he}} \right)}{\frac{V_c}{T_{ck}} + \gamma \left(\frac{V_k}{T_k} + \frac{V_r}{T_r} + \frac{V_h}{T_h} \right) + \frac{V_e}{T_{he}}} \tag{14}$$

In Eq. (15), the differential form of the mass equation in the compression chamber is given. Also, in Eqs. (16) and (17), the mass equation in heat exchangers (cooler, regenerator, heater) and expansion chamber are presented, respectively [44]:

$$dm_c = \frac{p dV_c + V_c \frac{dp}{\gamma}}{R T_{ck}} \tag{15}$$

$$m_i = \frac{p V_i}{R T_i}, i = k, r, h \tag{16}$$

$$m_e = M - (m_c + m_k + m_r + m_h) \tag{17}$$

In Eq. (18), the mass differential equation in heat exchangers is given, and also Eqs. (19) to (22) represent the mass flow in different parts of the SE. The dual subscripts denote the interference location of the five control volumes. For example, according to Fig. 3, the double index of ck indicates the flow at the boundary between the compression chamber and the cooler.

$$dm_i = \frac{m_i dp}{p}, i = k, r, h \tag{18}$$

$$m_{ck} = -dm_c \tag{19}$$

$$m_{kr} = m_{ck} - dm_k \tag{20}$$

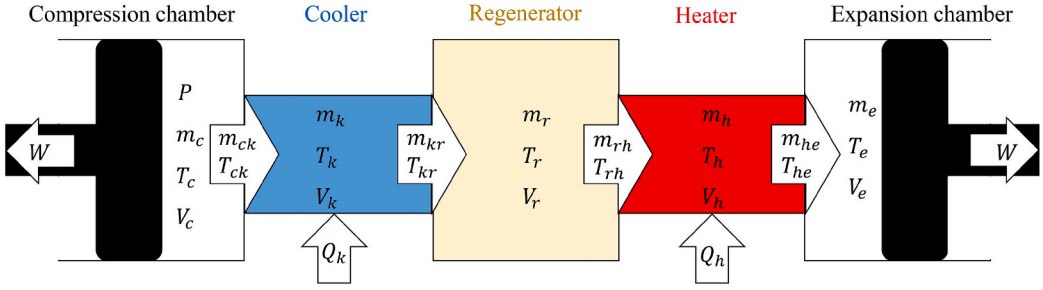

Fig. 3. SE components [44].

$$m_{rh} = m_{kr} - dm_r \tag{21}$$

$$m_{he} = m_{rh} - dm_h \tag{22}$$

Boundary conditions [44]:

If $m_{ck} > 0$ then: $T_{ck} = T_c$, otherwise: $T_{ck} = T_k$.

If $m_{he} > 0$ then: $T_{he} = T_h$, otherwise: $T_{he} = T_e$

The temperature equation for the expansion and compression chambers can be expressed as Eq. (23) [44]:

$$T_i = \frac{pV_i}{Rm_i}, i = e, c \tag{23}$$

In Eqs. (24) to (27), the heat rejected in the cooler, the heat exchanged in the regenerator, the heat absorbed in the heater and the work output are given in differential states [44]:

$$dQ_k = \frac{V_k dpC_v}{R} - C_p(T_{ck}m_{ck} - T_{kr}m_{kr}) \tag{24}$$

$$dQ_r = \frac{V_r dpC_v}{R} - C_p(T_{kr}m_{kr} - T_{rh}m_{rh}) \tag{25}$$

$$dQ_h = \frac{V_h dpC_v}{R} - C_p(T_{rh}m_{rh} - T_{he}m_{he}) \tag{26}$$

$$dW = p(dV_e + dV_c) \tag{27}$$

Also, the volume changes in the swept space of the expansion and compression chambers for alpha type SEs as a function of the crank angle have been calculated in Eqs. (28) and (29), respectively [45].

$$V_e = \frac{V_{swe}}{2}[1 + cos(\theta + \alpha)] \tag{28}$$

$$V_c = \frac{V_{swc}}{2}[1 + cos(\theta)] \tag{29}$$

Here, V_{swe} and V_{swc} are displacement volumes in the expansion and compression chambers, respectively. Also, θ and α are the crank angle and the phase angle of the piston of the expansion chamber relative to the piston of the compression chamber, respectively, and at default condition, α is usually considered 90 degrees [45].

In the following, the brake output power of the SE can be calculated by considering irreversibility according to Eq. (30) [44]:

$$P_{SE} = W\eta_{II}\frac{n_r}{60} \tag{30}$$

Here W, η_{II} and n_r are output work in reversible adiabatic mode, the second law efficiency and engine speed in rpm, respectively. It is noteworthy that the second law efficiency is based on some irreversibility such as: pressure drops due to piston friction, incomplete regenerator heat recovery, flow friction in the regenerator and piston speed.

Second law efficiency is presented by Eq. (31) [44]:

$$\eta_{II} = \eta_{II,irr(1-\varepsilon_r)}\,\eta_{II,irr(\Delta p)} \tag{31}$$

In Eq. (31), $\eta_{II,irr(1-\varepsilon_r)}$ and $\eta_{II,irr(\Delta p)}$ are the effects of regenerator incomplete heat recovery and the effects of pressure drop in the engine, respectively. These two irreversibility parameters are defined in Eqs. (32) and (33), respectively [44]:

$$\eta_{II,irr(1-\varepsilon_r)} = \frac{1}{1 + \left(\frac{1-\varepsilon_r}{(\gamma-1)ln\lambda}\right) \bullet \eta_{Ideal}} \tag{32}$$

$$\eta_{II,irr(\Delta p)} = 1 - \frac{3\beta \bullet \frac{\Delta p_t}{p_1}}{\eta^* \bullet \left(\frac{T_h}{T_k}\right) \bullet ln\lambda} \tag{33}$$

$$\lambda = \frac{V_{max}}{V_{min}} \tag{34}$$

$$\eta_{Ideal} = \frac{W}{Q_h} \tag{35}$$

$$\beta = 1 - \frac{1}{3\lambda} \tag{36}$$

$$\eta^* = \eta_{Ideal} \bullet \eta_{II,irr(1-\varepsilon_r)} \tag{37}$$

$$T_h = T_{wh} - 45 \tag{38}$$

$$T_k = T_{wk} + 5 \tag{39}$$

Here, ε_r, γ, λ, η_{Ideal}, T_{wh}, T_{wk}, T_h, and T_k are the regenerator effectiveness coefficient, specific heat ratio, volume ratio, reversible adiabatic efficiency, heater wall temperature, the cooler wall temperature, the temperature of the gas inside the heater and the temperature of the gas inside the cooler. Also, p_1 and Δp_t are the inlet pressure and total pressure drop in the SE, respectively. They are defined according to Eqs. (40) and (41), respectively [44].

$$p_1 = \frac{4p_m}{(\lambda + 1)(\tau + 1)} \tag{40}$$

$$\Delta p_t = \Delta p_r + \Delta p_f + \Delta p_w \tag{41}$$

$$\tau = \frac{T_h}{T_k} \tag{42}$$

Here, p_m is average engine pressure and τ is the temperature ratio. Also, Δp_r, Δp_f and Δp_w express respectively the pressure drops due to the friction of gas in the regenerator, the movement of the piston in the cylinder and piston speed. They are evaluated according to Eqs. (43) to (45) [44].

$$\Delta p_r = \frac{2f\mu V_r G L_{reg}}{m_r D_{hr}^2} \tag{43}$$

$$\Delta p_f = \frac{(0.94 + 0.0015sn_r) \bullet 10^5}{3\beta}\left(1 - \frac{1}{\lambda}\right) \tag{44}$$

$$\Delta p_w = \left(\frac{sn_r}{60}\right) \bullet p_1 \left(\frac{\lambda \bullet ln\lambda}{\lambda - 1}\right) \sqrt{\frac{\gamma}{RT_k}}\left[1 + \sqrt{\frac{T_h}{T_k}}\right] \tag{45}$$

In Eqs. (43) to (45), f, μ, V_r, L_{reg}, G, m_r, D_{hr} and s are the regenerator frictional coefficient, gas viscosity, regenerator volume, regenerator length, gas mass flow per unit area, regenerator gas mass, hydraulic diameter of the regenerator, and the stroke of the piston, respectively.

The dead volume of the regenerator is calculated by Eq. (46) [44].

$$V_r = n_{reg}\,\frac{\pi\, d_{reg}^{\,2}}{4}\,\varphi\, L_{reg} \tag{46}$$

Here n_{reg}, φ, d_{reg} are number of regenerators for each cylinder, porosity, and diameter of regenerator, respectively. Also, the regenerator hydraulic diameter is evaluated by Eqs. (47) and (48) [44]:

$$D_{hr} = \frac{4V_r}{A_{wg}} \tag{47}$$

$$D_{hr} = \frac{d_m\varphi}{(1 - \varphi)} \tag{48}$$

Here, A_{wg} and d_m are the wetted surface and the diameter of the wires inside the regenerator, respectively. In Eqs. (49) and (50), the wetted surface of the regenerator and the porosity coefficient in the regenerator are presented, respectively [44].

$$A_{wg} = \pi d_m L_m \tag{49}$$

$$\varphi = \frac{V_r}{(V_r + V_m)} \tag{50}$$

$$V_m = \frac{\pi d_m^{\ 2}}{4} L_m \tag{51}$$

Here, L_m and V_m are the total length and volume of the wires inside the regenerator, respectively.

Also, the frictional coefficient in the regenerator can be calculated from Eq. (52) [44]

$$f = 54 + 1.43 Re^{0.78} \tag{52}$$

Reynolds number in the regenerator can be calculated from Eq. (53) [44].

$$Re = \left| \frac{G D_{hr}}{\mu} \right| \tag{53}$$

The regenerator effectiveness is the important parameter in determining the efficiency of the heat regenerator and is defined by Eq. (54) [44].

$$\varepsilon_r = \frac{NTU}{NTU + 1} \tag{54}$$

Here, NTU represents the number of transfer units. It is defined according to Eq. (55) [44].

$$NTU = \frac{St\, A_{wg}}{A} \tag{55}$$

Here, A is the gas flow cross-sectional area in the regenerator. Also, the Stanton number in the regenerator is presented by St and is calculated according to Eq. (56) [44].

$$\mathrm{St} = 0.023\ \mathrm{Re}^{-0.2} \mathrm{Pr}^{-0.6} \tag{56}$$

Here, Pr is the dimensionless Prantel number.

Also, the brake thermal efficiency of the SE is calculated by Eq. (57) [44].

$$\eta_{th,SE} = \frac{P_{SE}}{\dot{m}_f LHV} \tag{57}$$

Here, $\dot{m}_f LHV$ is the thermal energy released due to the burning of natural gas in the external heat source of the SE and can be calculated by Eq. (58).

$$\dot{m}_f LHV = Q_h \frac{n_r}{60} \tag{58}$$

Also, the brake output torque of the SE is defined in Eq. (59) [45].

$$T_{SE} = \frac{9550\, P_{SE}}{Nr} \tag{59}$$

3. General simulation of CCHP system

3.1. Technical simulation

One of the appropriate technical analyzes for the CCHP system is to obtain a parameter that calculates the maximum utilization percentage of fuel energy input to the system, which is possible with the help of overall efficiency. So, the overall efficiency or CCHP efficiency of the CCHP system is given by Eq. (60) [46].

$$Overall\ Efficiency = \frac{Power + Heating + Cooling}{\dot{m}_f LHV} \tag{60}$$

In Eq. (60), power, cooling and heating loads are equal respectively to the output power of the whole system, the cooling and heating loads of the whole system and is calculated according to Eqs. (61) to (63).

$$Power = P_{ICE} + P_{SE} \tag{61}$$

$$Heating\ Load = Q_{cool} + \frac{Q_k}{2} \frac{n_r}{60} \tag{62}$$

$$Cooling\ load = (Q_{ex}\ COP_{ac}) + \left(\frac{Q_k}{2} \frac{n_r}{60} COP_{ac} \right) \tag{63}$$

It is obvious that the waste heat from the cooling system of the ICE and SE is utilized to supply the heating load, as well as the waste heat from the exhaust gases from the ICE and the rest part of the waste heat in the SE cooler is utilized to supply the required heat for the absorption chiller to provide required cooling power. Also, COP_{ac} is the coefficient of performance of the absorption chiller, and for a single-effect absorption chiller, COP_{ac} is usually around 0.7 [27,30].

Also, the electrical efficiency, heating efficiency, and cooling efficiency for the CCHP system are defined according to Eqs. (64) to (66), respectively.

$$Electrical\ Efficiency = \frac{Power}{\dot{m}_f LHV} \tag{64}$$

$$Heating\ Efficiency = \frac{Heating}{\dot{m}_f LHV} \tag{65}$$

$$Cooling\ Efficiency = \frac{Cooling}{\dot{m}_f LHV} \tag{66}$$

Another technical analysis to evaluate the CCHP systems is to compare these systems in terms of primary energy savings with a conventional energy supply system to provide the same amount of energy. By doing this comparison, the technical efficiency and the saving in the primary energy consumption (fuel consumption) of the CCHP system will be better determined, which will be discussed in the introducing of this parameter.

In a conventional system for buildings, electrical energy is supplied from thermal power plants, and an electric-driven chiller and a gas boiler are usually used to provide cooling and heating. Thus, if the conventional system supplies the same energy as the CCHP system, its primary energy consumption is calculated according to Eq.(67) [47].

$$PE_{conv} = \frac{Power\ \eta_g}{\eta_{el}} + \frac{Heating\ Load}{\eta_b} + \frac{Cooling\ Load}{\eta_{el} COP_{el}} \tag{67}$$

where η_{el}, η_g, η_b and COP_{el} are, respectively, the electric efficiency of the power plant, the efficiency of the electric generator, the gas boiler efficiency and the COP of the electric compression chiller. Their values are equal to 0.3, 0.9, 08 and 3, respectively [32].

Also, for the proposed system, the amount of primary energy consumption, PE_{CCHP}, is obtained according to Eq.(68).

$$PE_{CCHP} = \dot{m}_f LHV \tag{68}$$

The percentage of primary energy savings (PES) of the CCHP system compared to the conventional energy supply system is obtained by Eq. (69) [47].

$$PES = \left(\frac{PE_{conv} - PE_{CCHP}}{PE_{conv}} \right) 100 \tag{69}$$

where PE_{conv} denotes the amount of primary energy consumption for the considered conventional system.

Considering that both prime movers in this study operate based on the heat potential of natural gas, it can be useful to calculate the specific fuel consumption of natural gas. Therefore, the power specific fuel consumption (PSFC) and the overall specific fuel consumption (OSFC) of the CCHP system are given by Eqs. (70) and (71).

$$PSFC = \frac{\dot{m}_f}{Power} \tag{70}$$

$$OSFC = \frac{\dot{m}_f}{Power + Heating\ Load + Cooling\ Load} \tag{71}$$

3.2. Economic simulation

One of the appropriate methods in economic analysis is to calculate the project's investment payback period (IPP). In this model, the evaluation criterion is the time that should be spent to compensate the initial costs of the project (investment cost) with annual profit. In this way, in Eq. (72), the simple payback period (SPP) of the CCHP system is presented [5].

$$SPP = \frac{C_0}{ACS} \tag{72}$$

Here, C_0 is the investment costs (initial costs) of the CCHP system, and the ACS parameter is the annual cost saving or annual profit of the system. It is obvious that the economic inflation rate is not considered in the evaluation of the simple IPP. Economic inflation leads to a longer IPP, and it is better to include the economic inflation rate in the evaluation of the IPP. Thus, the discounted payback period (DPP) is defined in Eq. (73) [5].

$$DPP = \frac{ln\left(\frac{ACS}{ACS - C_0 r}\right)}{ln(1+r)} \tag{73}$$

Here r is the annual inflation rate.

In the following, the calculation method for the amount of annual cost saving (ACS) is given. It is obvious that both prime movers of the CCHP system of this study use natural gas, and only natural gas is used to supply the heating, cooling and electrical loads. In this way, according to Eq. (74), the fuel cost of the CCHP system is presented [28].

$$Cost_{CCHP} = \dot{m}_f \, LHV \, Price_F \tag{74}$$

Here, $Price_F$ is the global price of buying natural gas and its price is around 1 cent/kWh [48]. Also, if a conventional energy supply system wants to supply the same amount of energy as the CCHP system, the fuel cost (primary energy cost) of the conventional system is calculated according to Eq. (75) [48].

$$Cost_{conv} = Price_W \, Power \, \eta_g + \frac{Price_F \, Heating \, Load}{\eta_b} + \frac{Price_W Cooling \, Load}{COP_{el}} \tag{75}$$

Here, $Price_W$ is the global electricity purchase price and its value is in the range of 13 cents/kWh [48]. The amount of annual profit or ACS of the CCHP system compared to a conventional energy supply system for the same energy supply is obtained according to Eq. (76) [48].

$$ACS = [Cost_{Conv} - Cost_{CCHP}] \times 365 \, ho \tag{76}$$

Here, ho is set to be 8 h and is the number of the system's daily operating hours.

3.3. Environmental assessment

In this study, an environmental assessment of the performance of the CCHP system has been conducted and the amount of carbon dioxide emission reduction as well as the carbon tax reduction from the CCHP system compared to the conventional energy supply system has been calculated according to Eqs. (77) and (78) [46]

$$CO_2ER = \frac{\left(mCO_2^{Conv} - mCO_2^{CCHP}\right)}{10^6} \times 365 \, ho \tag{77}$$

$$CO_2TR = \left(mCO_2^{Conv} - mCO_2^{CCHP}\right) \gamma_{CO2} \times 365 \, ho \tag{78}$$

Where γ_{CO2} is CO2 tax rate, and is equal with 0.00003 \$ g^{-1} [46].

Also, the amount of carbon dioxide emitted from the CCHP and conventional systems has been estimated using Eqs. (79) and (80).

$$mCO_2^{CCHP} = \mu CO_2^F \bullet \dot{m}_f \, LHV \tag{79}$$

$$mCO_2^{Conv} = \left[\mu CO_2^W \bullet Power \, \eta_g + \frac{\mu CO_2^F \bullet Heating \, Load}{\eta_b} + \frac{\mu CO_2^W \bullet Cooling \, Load}{COP_{el}}\right] \tag{80}$$

Here, μCO_2^F and μCO_2^W are the carbon dioxide emission indices for burning natural gas and generating electricity, and are equal to 220 gr/kWh and 836 gr/kWh respectively [46].

4. Optimization, solution and validation of the numerical model

In this section by using optimization algorithms, the desired design parameters (decision variables) can be selected in the optimal state with high accuracy. Thus, in this article, after carrying out technical and economic modeling for the proposed CCHP system, an optimal technical and economic performance size is proposed.

To find an optimal size of decision variables of the CCHP system, first the optimal Pareto front is calculated using the genetic algorithm, and then the best two-objective optimal point is considered with the help of the Linmap decision-making method, which in the following, genetic algorithm, decision-making method, decision-making variables and objective functions are discussed. Finally, in this section, the modeling and optimization method will be presented and validation will be performed.

4.1. Genetic algorithm, decision-making method and variables

In this study, genetic algorithm (GA) method is used for optimization. GA is one of the most reliable evolutionary algorithms to do optimization [49]. Also, multi-objective optimization problem is used for optimization which its solution includes a set of optimal solutions known as Pareto front. The NSGA-II algorithm is a widely used iterative, stochastic optimization method for solving multi-objective problems with conflicting goals. Instead of finding a single optimal solution, it identifies a set of optimal trade-offs known as the Pareto front, where each solution is best in at least one objective. The Pareto front is formed by selecting and evaluating random points, then identifying non-dominated solutions based on whether the objective is to minimize or maximize [50]. In this analysis, the algorithm used a crossover rate of 0.8, mutation rate of 0.1, and a population size of 160 to effectively explore and exploit the solution space.

The decision to employ GA was driven by its proven robustness and effectiveness in addressing complex, multi-objective optimization challenges. GA excels in navigating large and discontinuous solution spaces, leveraging its population-based search approach to explore multiple potential solutions concurrently. This capability is particularly valuable for identifying the Pareto front in multi-objective optimization, as it efficiently produces a diverse range of optimal solutions. Furthermore, GA's ability to manage non-linear and non-differentiable objective functions enhances its suitability for the specific problem under investigation. While other optimization techniques, such as PSO and GWO, are also highly effective, GA's adaptability in handling multiple objectives and its demonstrated success in comparable applications [51] made it the most appropriate choice for this study.

After achieving the optimal Pareto front, the optimal solution can be identified from the Pareto front with the help of Linmap decision making method [52]. In this method, finding the best solution from the Pareto front is based on the Euclidean distance of each solution to the ideal solution.

Decision variables (design parameters) for optimization in the present work are as follows: SE speed, regenerator length, regenerator porosity, SE phase angle, and ICE parameters, including engine speed, spark start angle, and combustion angle duration. These parameters are presented below according to their limitation range.

$$\text{Decision making variables}: \left\{ \begin{array}{c} 1000 \le n_r \le 6000 \text{ rpm} \\ 19 \le L_r \le 50 \text{ mm} \\ 0.6 \le \varphi \le 0.9 \\ 80 \le \alpha \le 140 \text{ deg} \\ 1000 \le N_r \le 6000 \text{ rpm} \\ 320 \le \theta_s \le 350 \text{ deg} \\ 35 \le \theta_d \le 45 \text{ deg} \end{array} \right\}$$

The technical and economic functions of the two-objective form are the CCHP efficiency and the IPP of the system. The CCHP efficiency should be maximized, and the IPP should be minimized.

4.2. ICE and SE simulation method and optimization method

In order to solve the differential equations of the dimensionless initial value of the ICE (Eqs. (1) to (4)), the fourth-order Runge-Kutta numerical method has been utilized. The initial values of dimensionless parameters of the pressure, net-work, heat dissipation, and gas mass at the start of the compression stage are respectively 1, 0, 0, and 1. The range of solving the problem is from $\theta = -180^\circ$ to $\theta = 180^\circ$ (the beginning of the compression process to the end of the combustion). In the MATLAB environment, the final value of these dimensionless parameters is obtained at the end of the combustion stage ($\theta = 180^\circ$) and then the values are calculated with their dimensions.

The differential equations of the reversible adiabatic model (Eqs. (14) to (27)) are solved in the MATLAB software with the first-order Runge-Kutta method with the help of a developed computer program. The value of 0.1 degrees is considered as the angular step. The maximum iteration number is 50. The condition of the convergence for pressure is 1 kPa. After solving the reversible or ideal adiabatic relations, irreversibilities are considered.

In this study, optimization has been performed using the genetic algorithm by the MATLAB software. The initial population size is set to be 160. Also, the probability of intersection and the probability of mutation are 0.8, and 0.1, respectively. The termination condition is defined as an error difference value of 0.001 between two consecutive iterations. Fig. 4 shows the modeling and optimization solution steps for this study.

4.3. SE and ICE model validation

In this section, the validity of the simulation is discussed. In this way, the results of the current work used to simulate the SE and the ICE are compared by experimental results and other models, and then the validation of the numerical model used for the heat recovery system is discussed.

To confirm the accuracy of the SE simulation, the geometrical characteristics of the well-known GPU-3 engine have been used, and a lot of research has been done on the modeling and optimization of this engine. This engine is one of the successful engines manufactured by General Motors. It is a beta-type single-cylinder Stirling engine, where the power and displacer pistons are built into one cylinder (Fig. 5) [45]. Also, the technical specifications of this engine can be seen in Table 2.

In Table 3, the output power and thermal efficiency of the GPU-3 engine at 2500 rpm, working pressure of 4.14 MPa, heater temperature of 977 K, and cooler temperatures of 288 K, with helium as working gas, have been calculated using the irreversible adiabatic model. The results obtained in the current work have been compared with the results of other numerical modeling and experimental data.

In the present research, the development of Costea et al. [54] model has been developed. Instead of mathematical solution, the assumptions of the adiabatic model are used, and the ideal adiabatic differential equations are solved by Range-Kutta method. Then, similar to their model [54], by considering frictional irreversibilities such as piston friction in the cylinder, flow friction in the regenerator, and pressure drops as well as thermal irreversibilities such as non-ideal heat recovery

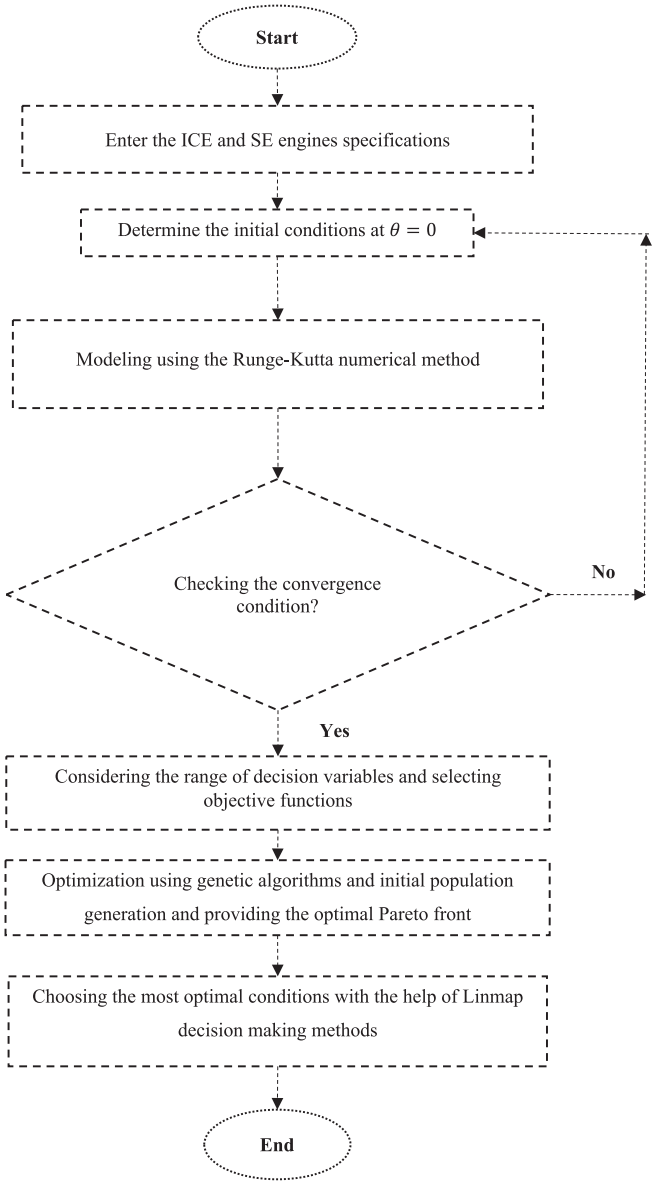

Fig. 4. Modeling and optimization solution steps.

in the regenerator, the efficiency of the second law is evaluated and with the help of reversible adiabatic efficiency, the brake output power and efficiency are calculated. The current model errors in predicting the power and thermal efficiency are 5 % and 4.28 %, respectively which is on average, higher accuracy than previous research.

In this research, the model used to simulate the ICE is a zero-dimensional model that is solved numerically. To ensure the accuracy of the model, the results are compared by the experimental results of the EF7 engine.

The EF7 engine (Iranian National Engine) is an in-line 4-cylinder engine. It is designed to operate on natural gas fuel and also it has the ability to work with gasoline (Fig. 6) [27]. The technical specifications of this engine are presented in Table 4.

In Fig. 7a, the brake output torque from the EF7 engine is modeled using the current model, the Kakai and Karimi model [65], and the experimental tests [65]. In Ref. [65], one-dimensional GT-Power commercial software was used for engine modeling. The maximum deviation between the present work and the model of Kakai and Karimi in predicting the output torque is lower than 4 %. However, as it is clear from Fig. 7a, the benefit of the present model can be attributed to the

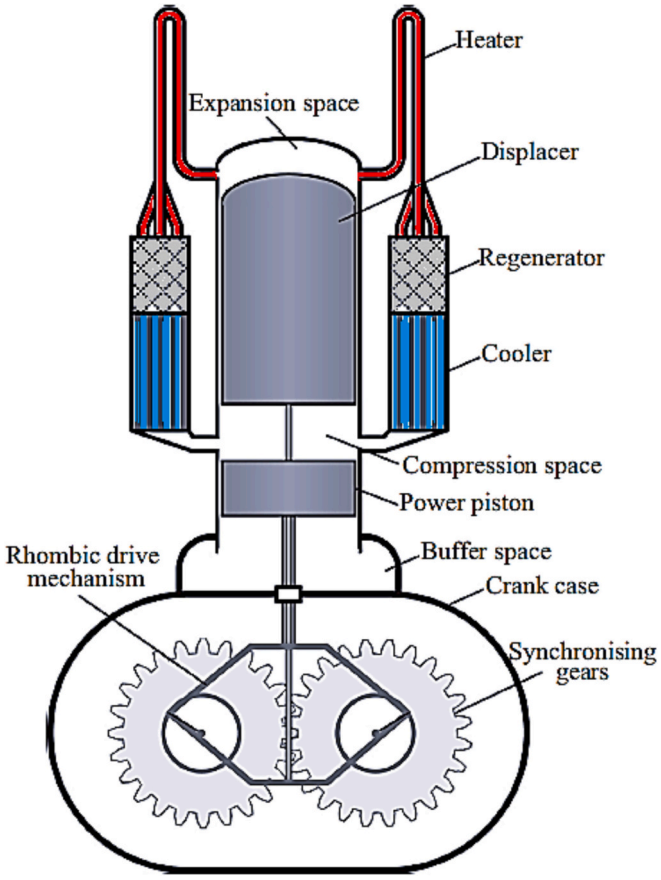

Fig. 5. The schematic diagram of the GPU-3 engine [53].

Table 2
The GPU-3 engine's dimension characteristics [45].

Characteristic	Value	Characteristic	Value
Working gas	Helium	Length of tube	245.3 mm
Max. mean pressure	6.9 MPa	Cooler	
Clearance volumes		Number of tubes	312
Expansion space	30.52 cm^3	Inside diameter of the tube	1.09 mm
Compression space	28.68 cm^3	Length of tube	46.1 mm
Swept volumes		Regenerator	
Expansion space	120.82 cm^3	Internal diameter	22.6 mm
Compression space	113.14 cm^3	Length	22.6 mm
Internal diameter of cylinder	69.9 mm	Matrix wire diameter	40 μm
Heater		Porosity	0.697
Tubes number/cylinder	40	Matrix mesh size	79
Tube inner diameter	3.02 mm	Number of regenerators/ cylinders	8

potential of finding the optimal engine speed (4000 rpm) in order to maximize the torque, while the model of Ref. [65] does not predict with adequate accuracy.

Also, in Fig. 7b, the output power of the present model for the EF7 engine at different speeds has been modeled and compared with the results of experimental tests [66]. According to the results of Fig. 7b, it is clear that the current model has high accuracy in estimating the output power for the internal combustion engine and the highest model error for predicting power is reported to be less than 4 % at high speeds.

Table 3
Validation of the current model with GPU-3 engine results.

Type of model	P_b (kW)	η_b (%)	P_b error (%)	η_b error (%)
Urielli and Berchowitz [45] (Ideal adiabatic model)	8.3	62.5	109.6	78.5
Urielli and Berchowitz [45] (Simple model)	6.7	52.5	69.20	50
Formosa and Despesse [55]	6.08	52.9	53.5	51.1
Ahmadi et al. [56]	4.8	29.27	21.2	16.4
Timoumi et al. [57]	4.27	38.49	7.8	10
Ni et al. [58]	4.22	33	6.6	5.7
Ahmed et al. [59]	4.507	36.56	13.8	4.4
Toghyani et al. [60]	4.17	36.2	5.3	3.4
Bataineh [61]	4.12	39.5	4.05	12.9
Hosseinzade and Sayyaadi [62]	4.11	36.2	3.78	3.42
El-Ghafour et al. [63]	4.05	36.05	2.27	3
Current model	**3.94**	**33.5**	**0.5**	**4.28**
Experimental [45,55–63]	3.96	35		

5. Results of simulation and optimization

As described, in this CCHP arrangement, the prime movers of the EF7 and the Ford-Phillips engines are used in a hybrid form. Also, the specifications of the Ford-Phillips SE and the costs of the components of the CCHP system are presented in Tables 5 and 6, respectively. The total cost of the components of this arrangement is estimated at $ 178,300.

In this part, the influence of the parameters of the SE and the ICE on the performances of the CCHP system is analyzed. The working pressure of the SE is 10 MPa, the input energy of the SE is obtained from the burning of natural gas, and the fuel consumed by the ICE is natural gas.

5.1. Effect of the Stirling engine's parameters

5.1.1. SE speed

As the thermal energy input to the Stirling engine (SE) heater increases, the engine speed increases, and as the engine speed increases, the engine power and capacity are enhanced. However, on the other hand, increasing the engine speed causes increased friction and heat losses in various parts of the engine, which can have negative effects on energy efficiency. Thus, it is better to carefully examine the effect of this parameter on the performance of the entire system.

In Fig. 8a, the influence of the SE speed on the capacity (power, heating and cooling loads) of the CCHP system based on the ICE and SE is investigated. It is noteworthy that all other specifications of SE and ICE are default during parametric analysis and the ICE speed is considered to be 3500 rpm. By increasing the SE speed to 3700 rpm, the maximum output power of the system can be achieved in the range of 118.41 kW, and after that, the decrease of power occurs because of the rise of irreversibility. Also, the system heating and cooling capacities always increases with the increase in the SE speed.

In Fig. 8b, the influence of the SE speed on the overall efficiency and percentage of PES of the CCHP system is modeled. Considering that at low speeds, SEs usually have a good thermal efficiency, so in this range the overall efficiency will reach its maximum value of about 79 %. Also, the highest amount of PES at 1000 rpm is reported in the range of 38 %. However, at speeds higher than 5500 rpm, because the output power drops and the SE has low efficiency, there is no saving in the primary energy consumption, and the value of PES becomes negative. So in this state, the consumption of primary energy of the CCHP system is greater than that of the conventional system.

Also, if the CCHP system based on the Ford-Phillips SE is started alone at high speeds (for example, at 4500 rpm), the overall efficiency of the CCHP system is about 57 % [35]. By using the hybrid CCHP system arrangement of this study, due to the introduction of the ICE, the overall efficiency will reach nearly 64 %, at 4500 rpm for the SE, according to Fig. 8b, which is strengthened by about 12 % compared to the overall

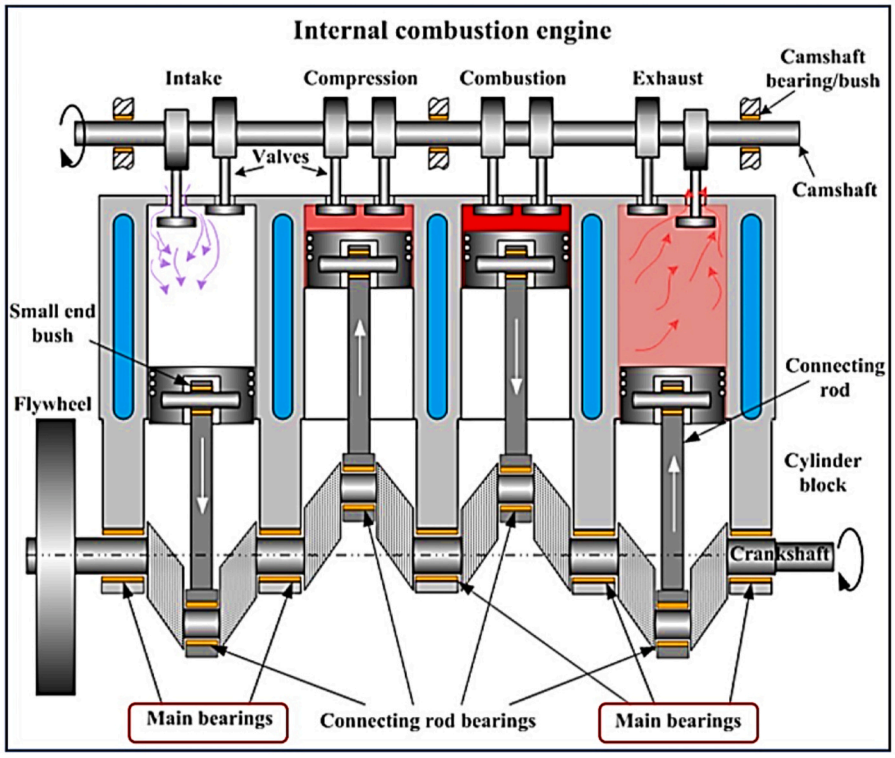

Fig. 6. Schematic of the EF7 combustion engine [64].

Table 4
EF7 engine specifications [27].

Parameter	Value	Parameter	Value
Cylinder numbers	4	Combustion start	326 deg
Piston stroke	85 mm	Combustion duration	40 deg
Displacement volume	1645 cm^3	Rotational speed range	1000–6000 rpm
Cylinder bore	78.6 mm	Engine compression ratio	11.2

efficiency of the standalone SE reported in Ref. [35]. Therefore, the use of this CCHP arrangement has a more appropriate technical performance at high SE speeds compared to Ref. [35].

In Fig. 8c, the power specific fuel consumption (PSFC) and the overall specific fuel consumption (OSFC) of the CCHP system are simulated at different speeds of the SE. It is clear that the PSFC is a reasonable value at low speeds and grows at a high rate with increasing speed due to the increase in losses, so that at 6000 rpm the PSFC is about twice as much as at low speeds. However, because in calculating the OSFC, in addition to power, the heating and cooling loads also have an effect, and the heating and cooling loads always increase with increasing speed, at 6000 rpm the OSFC of the CCHP system has grown by less than 50 % compared to its low speeds.

Fig. 8d illustrates the discounted payback period (DPP) of the CCHP system with hybrid prime movers at different speeds of the SE, considering different rates for economic inflation. It is known that the shortest DPP is always obtained at 3700 rpm, so without considering inflation, the DPP is within 4.4 years. Also considering the average annual inflation of 8 %, the DPP reached to 5.62 years.

It is noteworthy according to the results of Ref. [35], if the CCHP system is used based on the Ford-Phillips SE alone at 3700 rpm, the DPP without considering inflation is about 3.15 years. By using a hybrid CCHP system arrangement (the model of this research), it has a weaker economic performance due to the relative high cost of the ICE, and the payback period is extended by about 1.25 years.

Also, according to Fig. 9, the effect of SE speed on the electrical

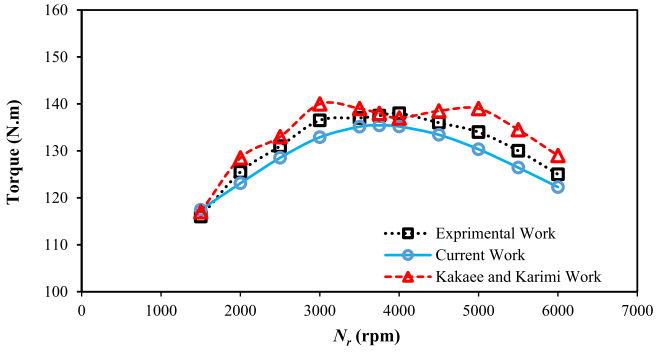

(a)

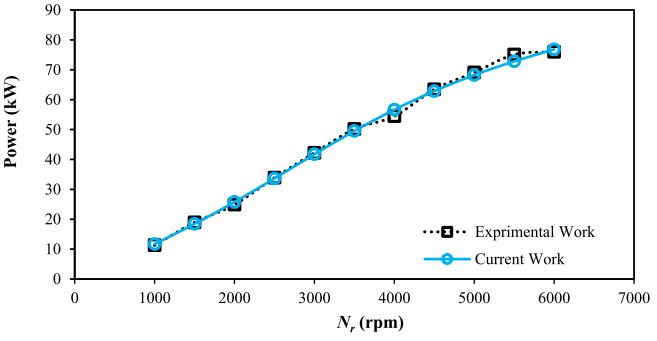

(b)

Fig. 7. (a) Comparing the brake output torque of the current model with the results of the Kakai and Karimi model [65], and the experimental tests [65], and (b) Comparing the brake output power of the current model with the results of the experimental tests [66].

Table 5
The Ford-Philips SE characteristics [35].

Characteristic	Value	Characteristic	Value
Working gas	Hydrogen	Length of tube	462 mm
Max. mean pressure	20 MPa	Cooler	
Clearance volumes		Number of tubes	742
Expansion space	214.2 cm^3	Inside diameter of tube	0.9 mm
Compression space	214.2 cm^3	Length of tube	87 mm
Swept volumes		Regenerator	
Expansion space	870.6 cm^3	Internal diameter	73 mm
Compression space	870.6 cm^3	Length	34 mm
Internal diameter of cylinder	73 mm	Matrix wire diameter	36 μm
Heater		Porosity	0.62
Tube inner diameter	4 mm	Matrix mesh size	200
Tubes number/cylinder	22	Number of regenerators/ cylinders	2

Table 6
CCHP system equipment purchase price [28,35].

Equipment	Price ($/kW)
SE	300
ICE	1180
Heat exchanger	25
Electric generator	40
Absorption chiller	160

efficiency, heating efficiency and cooling efficiency of the CCHP system is presented. As the speed of the SE increases, the pressure drop in the regenerator and cylinder of the SE increases, and a smaller percentage of the heat energy entering the engine is converted into output power, so the electrical efficiency always decreases as the speed of the SE increases. However, the increase in pressure drop in the SE does not have much effect on the heat output from the SE, and the heating and cooling efficiency does not change much as the engine speed increases.

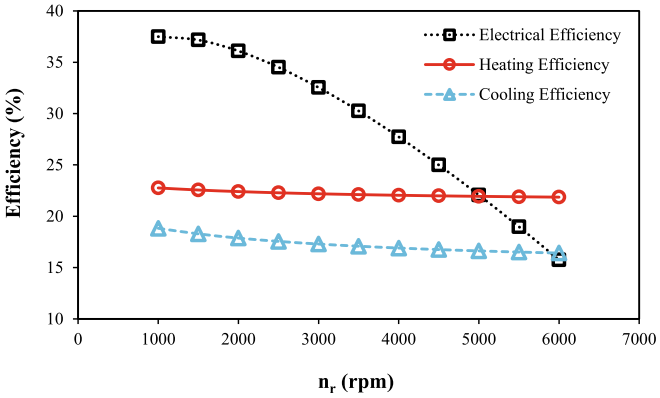

Fig. 9. The effect of the SE speed on the electrical, heating and cooling efficiencies of the CCHP system.

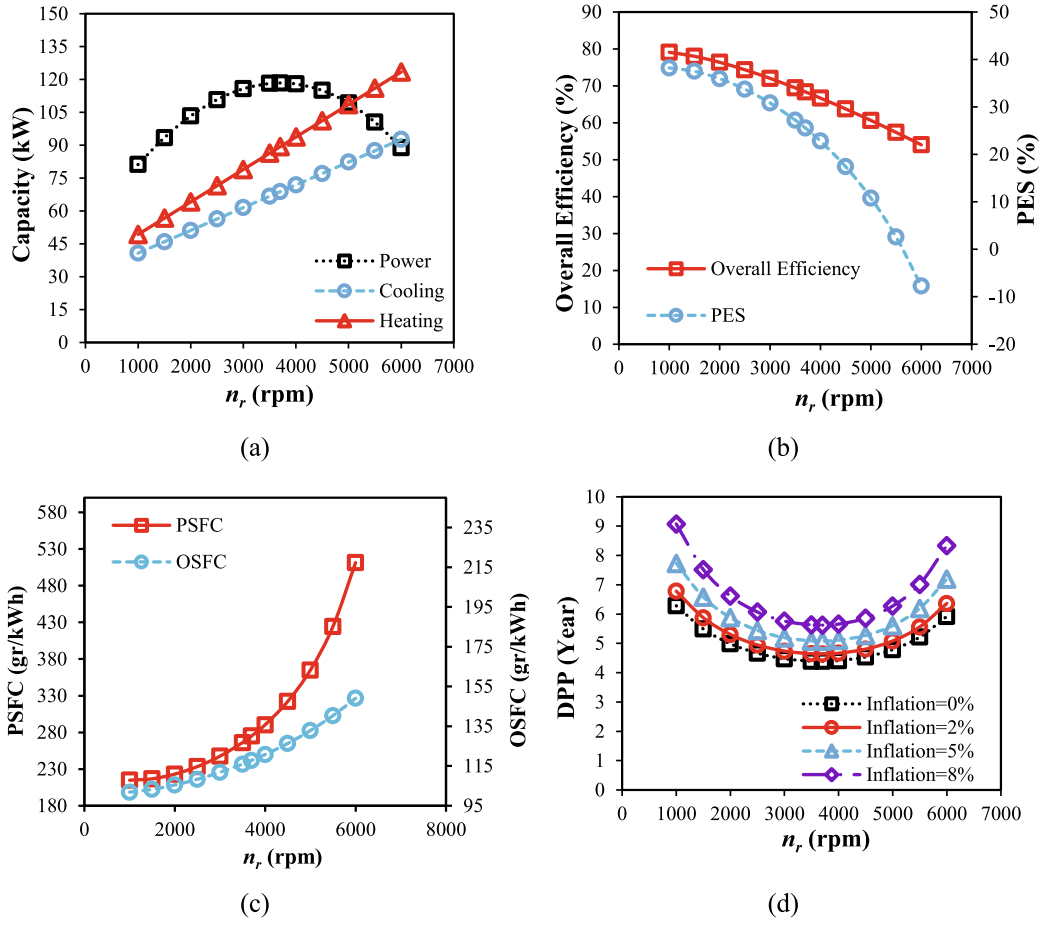

Fig. 8. (a) The effect of the SE speed on CCHP system's capacity, (b) The effect of the SE speed on CCHP efficiency and PES (c) The effect of the SE speed on PSFC and OSFC and (d) The effect of the SE speed on the discounted payback period of the CCHP system at different economic inflation rates.

5.1.2. SE phase angle

Increasing the phase angle on the one hand increases heat recovery and on the other hand, decreases the compression ratio and engine pressure. Therefore, increasing this parameter (phase angle) has opposite effects on the engine performance and it is better to choose its optimal ranges carefully according to the desired goals.

In Fig. 10a, the effect of the SE phase angle on the capacity (power, heating and cooling loads) of the CCHP system is investigated. It is noteworthy that all the parameters of the two engines are in default conditions, and the speed of the SE and ICE are considered to be 3500 rpm, and only the phase angle of the SE changes. During the operation of the SE, the volume changes of the expansion space must be ahead of that of the compression space, which is defined by the phase angle between the piston of the expansion and compression chambers. In default conditions, the phase angle of Ford-Phillips SE is 90 degrees. It is noteworthy that the phase angle in double-acting SEs can be changed with the help of the phase angle controller mechanism and its optimal value is determined according to the objectives of the problem [67–69]. Usually, the optimal value of the phase angle for SEs is 90 degrees [67–69].

In the phase angle range of 87 degrees, because the engine compression ratio is a suitable value, it is possible to achieve the maximum output power of 118.29 kW. Also, with further reduction of the phase angle to the range of 83 degrees, due to the shortening of the thermal recovery duration, the system heating and cooling capacities reach their maximum value of 86.8 kW and 67.03 kW, respectively.

In Fig. 10b, the overall efficiency and percentage of PES in different phase angles are simulated. As the phase angle increases, the thermal recovery duration in the regenerator increases and the overall efficiency and saving in primary energy consumption for the system always increases. It is obvious that the CCHP system technically performs better at high-phase angles.

Fig. 10c shows the effect of the SE phase angle on the DPP of the CCHP system, considering economic inflation. Because the maximum output power is within the phase angle of 90 degrees, it is possible to achieve the maximum amount of savings in annual costs and the shortest DPP, so in this condition, regardless of inflation, the DPP is equal to 4.4 years. When considering an inflation of 8 %, the DPP reaches about 5.63 years (Fig. 10c). From an economic point of view, the phase angle of about 90 degrees for the SE is more suitable for the CCHP system.

5.1.3. SE regenerator porosity

On the one hand, increasing the porosity coefficient increases the hydraulic diameter of the regenerator and reduces the pressure drop. On the other hand, the increase of this parameter causes the reduction of the heat transfer surface for recovery (reducing the effectiveness of the regenerator) and the increase of dead volume (reduction of engine pressure). Therefore, increasing this parameter can cause positive and negative performance in the power and efficiency of the system, and achieving its optimal value is very valuable.

In Fig. 11a, the influence of the regenerator porosity coefficient on the CCHP system capacity is given. In this way, the optimal value of the porosity coefficient to achieve the maximum amount of power according to Fig. 11a has been reported in the range of 0.68, and the amount of power in this condition reaches 123.5 kW. Also, an increase in the

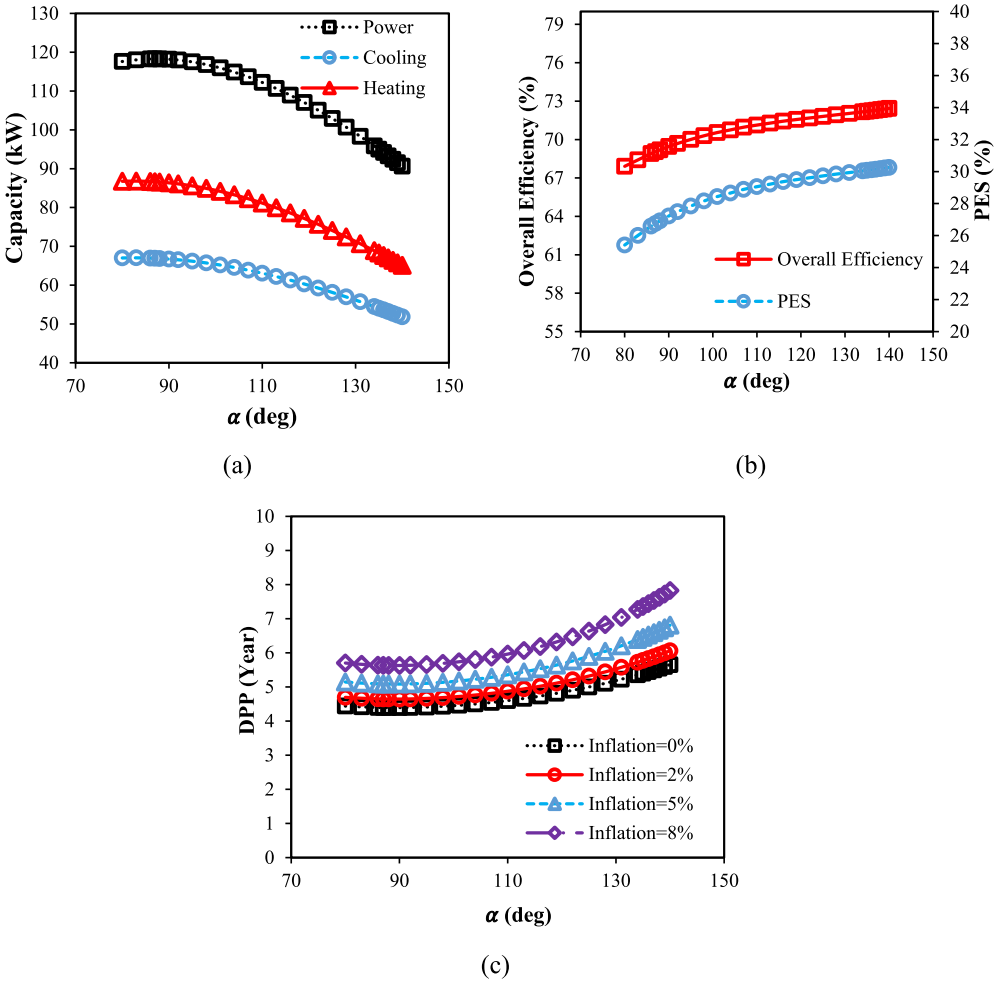

Fig. 10. (a) The effect of SE phase angle on the CCHP system capacity, (b) The effect of SE phase angle on the overall efficiency and PES and (c) The effect of the phase angle on the DPP of the CCHP system.

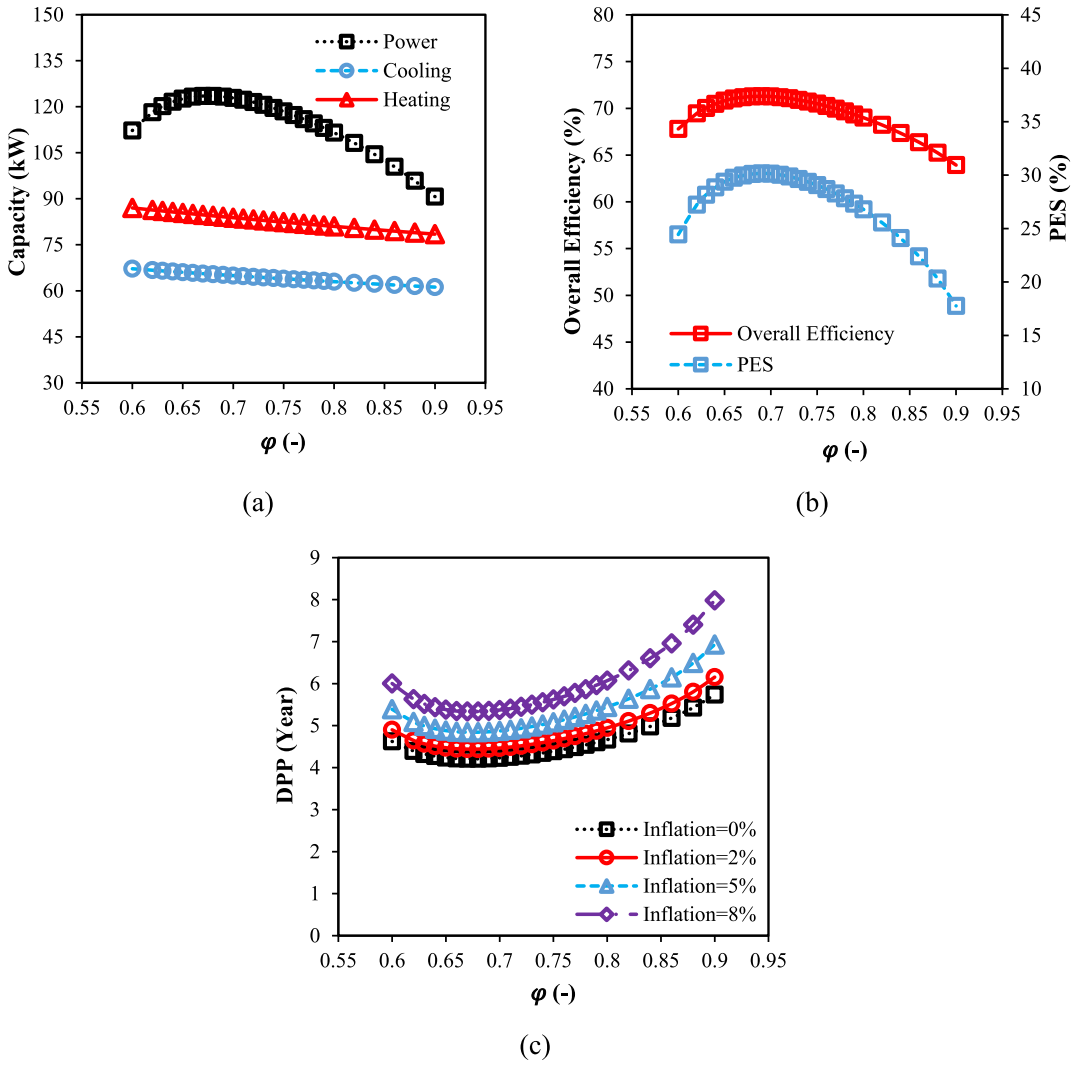

Fig. 11. (a) The influence of regenerator porosity coefficient on the CCHP system capacity, (b) The influence of regenerator porosity coefficient on the overall efficiency and PES and (c) The influence of the regenerator porosity coefficient on the DPP of the CCHP system.

porosity coefficient due to increased dead volumes, reduces engine pressure and capacity, and can reduce the heating and cooling loads (Fig. 11a).

According to Fig. 11b, the optimal porosity coefficient to achieve the highest values of the overall efficiency and the PES for the system is 69 % and the selection of this range of the porosity coefficient is technically more suitable for the CCHP system.

Fig. 11c shows the effect of the porosity coefficient on the DPP when considering the annual economic inflation. In the condition that the porosity coefficient is equal to 68 %, the capacity of the CCHP system gets a suitable value. Also, if economic inflation is not taken into account, the DPP is calculated as 4.21 years, and if the economic inflation rate is 8 %, the DPP is a little longer and reaches 5.33 years (Fig. 11c).

5.1.4. SE regenerator length

The rise of the regenerator length, on the one hand, increases the heat transfer surface for recovery (increasing the regenerator effectiveness) and increases the dead volumes of the engine (reducing the engine pressure). On the other hand, increasing this parameter can increase the flow friction in the regenerator. Therefore, increasing this parameter has multiple effects on the CCHP performance.

Fig. 12(a) shows the effect of the length of the regenerator on the capacity of the CCHP system. According to Fig. 12(a), the optimal length to reach the maximum power is in the range of 20 mm, and in this condition, the output power reaches 125.53 kW. Also, with the increase of the regenerator length, the heat recovery increases and the heat loss decreases. On the other hand, the dead volume increases and the engine pressure decreases. Eventually, an increment of the regenerator length reduces the heating and cooling loads.

In Fig. 12(b) the influence of the length of the regenerator on the overall efficiency and PES of the CCHP system is simulated. In the condition that the regenerator length is 26 mm, the maximum overall efficiency can be reached to the range of 69.8 %. Also, the highest percentage of PES is achieved when the length of the regenerator is equal to 28 mm. In this way, choosing the regenerator length in the range of 26 to 28 mm can be more appropriate for the CCHP system.

In Fig. 12(c), the influence of the length of regenerator on the DPP of the CCHP system is modeled by consider of the economic inflation. Always in the regenerator length of 20 mm, when the maximum amount of output power is obtained, the shortest DPP of the CCHP system is obtained, in such a way that without taking into account inflation and taking into account 8 % inflation, the DPP is calculated 4.11 and 5.19 years respectively.

5.2. Effect of the ICE'S parameters

5.2.1. ICE speed

At low speeds in internal combustion engines, a greater percentage of

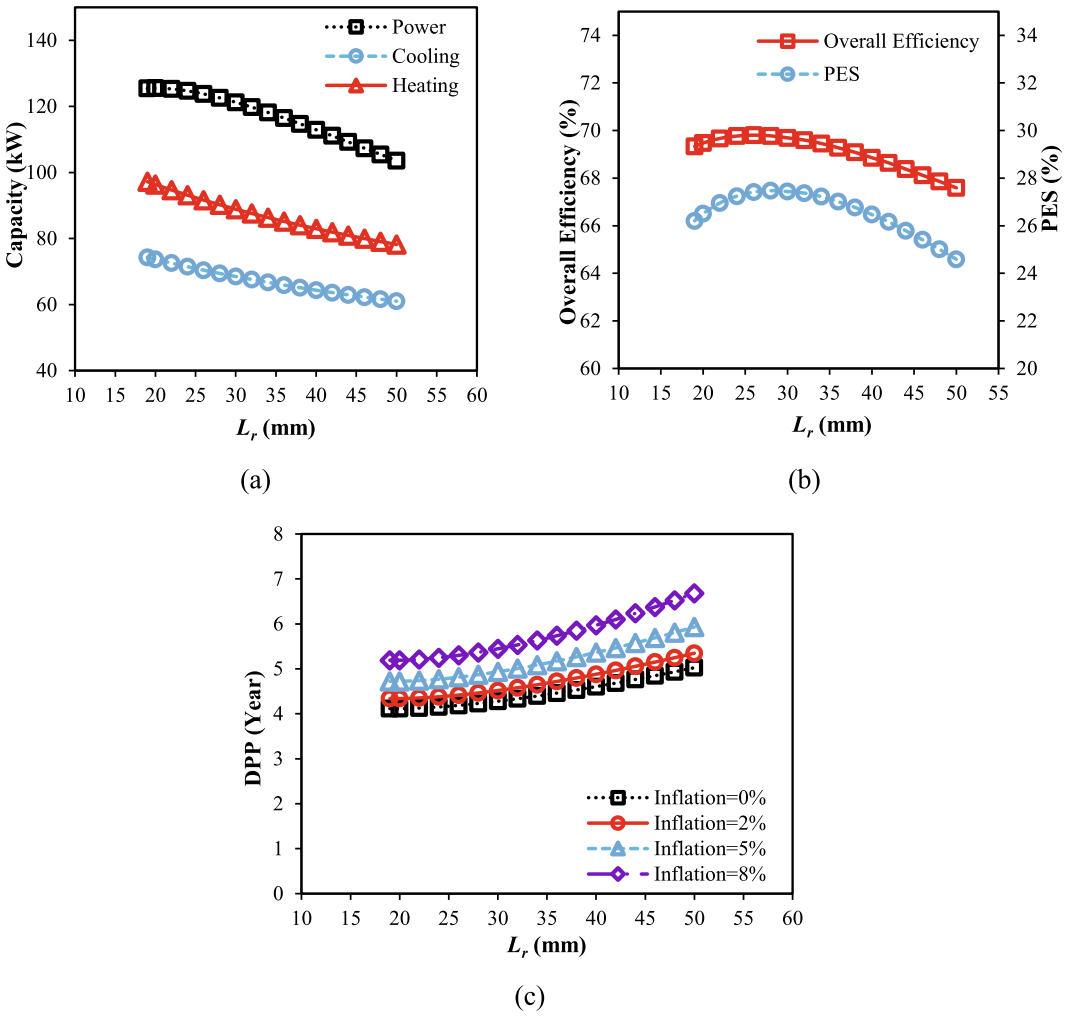

Fig. 12. (a) The influence of the length of regenerator on the CCHP system capacity, (b) The influence of the length of regenerator on the overall efficiency and PES, and (c) The influence of regenerator length on the DPP of the CCHP system.

the potential energy of the fuel input is lost through the engine walls, and at higher speeds, the effect of friction in various parts of the engine is more dominant, and determining the optimal speed is very important to achieve proper performance of these engines.

In the following, the influence of natural gas-powered ICE parameters on the CCHP performances is analyzed. It should be noted that the SE is set at a constant speed of 3500 rpm and in default conditions. In Fig. 13(a), the capacity of the CCHP system is presented at different ICE speeds. It shows that the system capacity increases with increasing engine speed. In Fig. 13(b) the overall efficiency and the PES of the CCHP system in various speeds of the ICE are presented. The optimal value of the ICE speed to achieve the highest value of the overall efficiency of the CCHP system is usually in the range of 4000 rpm, and the overall efficiency in this condition reaches nearly 70 %. Also, according to Fig. 13 (b), PES is maximized in the range of 3700 to 4000 rpm, and this range of ICE speeds for the system can be more suitable from a technical perspective.

In Fig. 13(c), the power specific fuel consumption (PSFC) and the overall specific fuel consumption (OSFC) of the CCHP system are modeled at different speeds of the ICE. The optimal value of the PSFC reaches its lowest value in the range of 266.07 g/kWh when the ICE is at 3700 rpm. It is noteworthy that since the heating and cooling loads increase with increasing engine speed, the optimal value of the ICE speed to achieve the lowest OSFC is usually slightly higher and in the range of 4000 rpm.

Fig. 13(d) gives the DPP of the CCHP system at various ICE speeds. Since the maximum amount of system capacity is achieved at high ICE speeds, the shortest DPP has been calculated in this range. Also, at 6000 rpm, without considering economic inflation and considering economic inflation of 8 %, the DPP is calculated as 3.5 and 4.28 years, respectively. So, the use of the CCHP system is economically more suitable in conditions where the ICE speed is high. It should also be noted that at 3500 rpm without considering economic inflation, the DPP of the CCHP system based on hybrid prime movers is 4.4 years (Fig. 13(d)). Also, in Ref. [28], the CCHP system which derived by a gas ICE alone, the simple payback period in this speed is nearly 6 years [28]. So, the model of this study (CCHP with hybrid primer movers) reduces the simple payback period by about 1.6 years compared to the CCHP system based on gas ICE [28]. Note that in the CCHP system arrangement of this study, the ICE and the Stirling engine were started in parallel, and each provided part of the power and energy required by the entire system. However, in the arrangement of Ref. [28], the combustion engine alone provided all the energy of CCHP system. It is clear that the price of the SE is much lower than the ICE according to Table 6, and in the conditions of Fig. 13 (d), the SE operates at 3500 rpm and has a suitable capacity considering its price, which ultimately shortens the payback period of the system. Therefore, using this arrangement of the CCHP system has a more suitable economic performance compared to Ref. [28].

Also, according to Fig. 14, the influence of ICE speed on the electrical efficiency, heating efficiency and cooling efficiency of the CCHP system

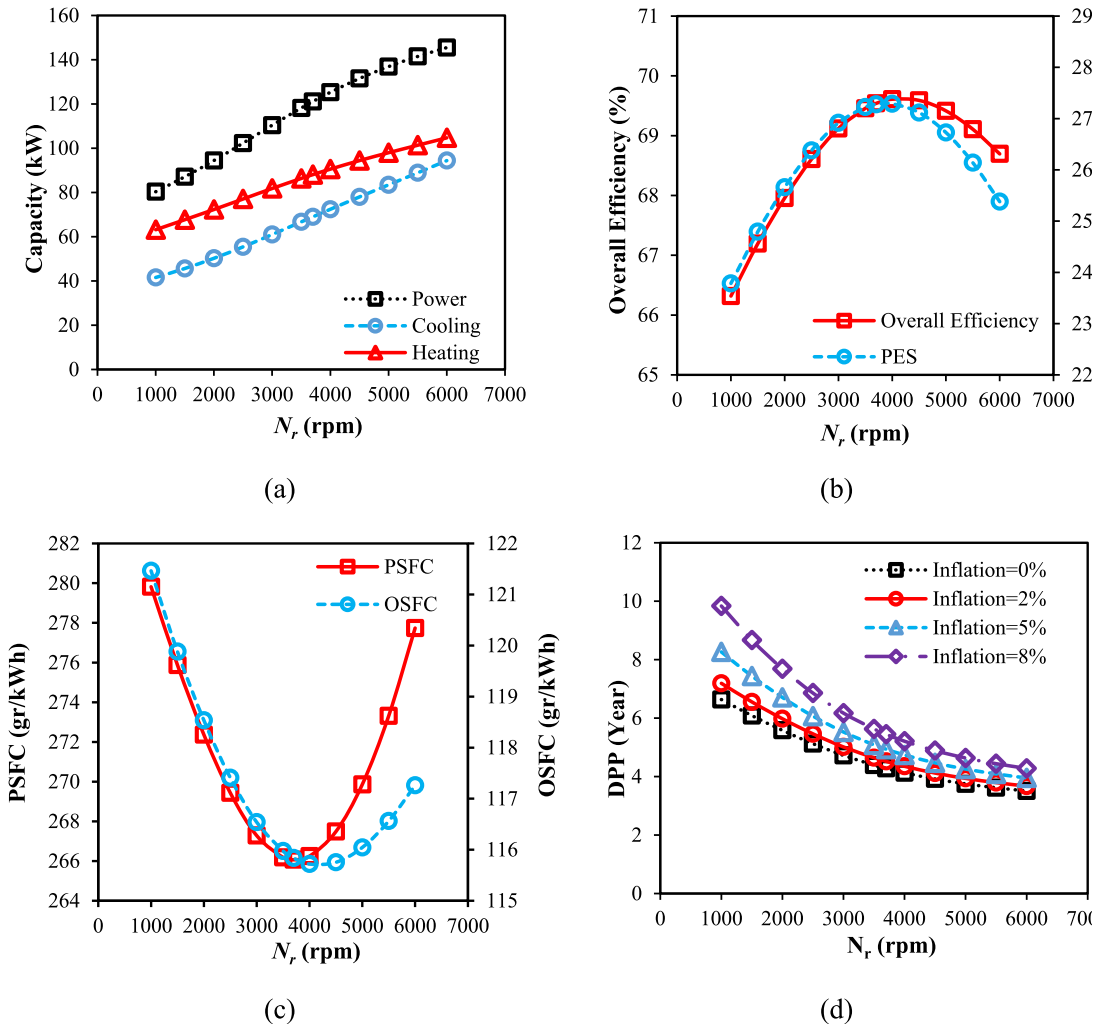

Fig. 13. (a) The influence of ICE speed on CCHP system capacity, (b) The influence of ICE speed on overall efficiency and PES, (c) The influence of ICE speed on PSFC and OSFC, and (d) The effect of ICE speed on the CCHP system DPP.

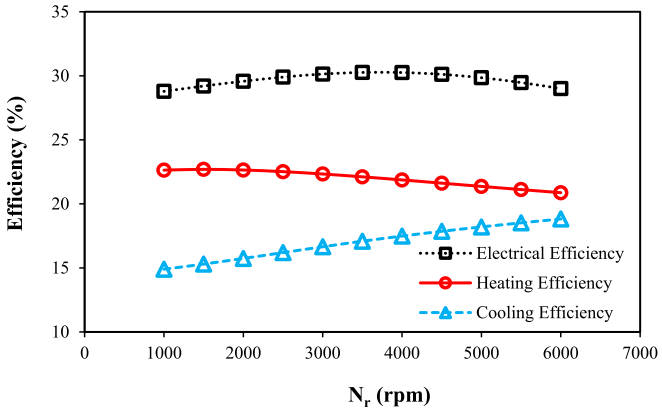

Fig. 14. The influence of ICE speed on the electrical, heating and cooling efficiencies of the CCHP system.

is modeled. Given that in the middle ICE speeds (around 3500 rpm) a smaller percentage of the thermal energy from combustion is released through the engine wall and in this condition the friction in different parts of the engine is not very high, in this condition the highest electrical efficiency of more than 30 % is achieved. It is also clear that as the engine speed increases, a smaller percentage of the energy from combustion is released through the engine wall and the heating efficiency decreases with increasing ICE speed. On the other hand, since increasing ICE speed causes the gases temperature from combustion to increase and the heat output from the ICE always increases, the cooling efficiency always increases with increasing engine speed (Fig. 14).

5.2.2. *ICE ignition parameters*

It is noteworthy that at high speeds, the spark must be fired a little earlier than the scheduled time (the spark timing should be advanced) so that the fuel in the cylinders burns on time and maximum power and thermal efficiency is achieved. On the other hand, advancing the spark timing too much can increase heat losses and reduce the engine's power and thermal efficiency. Also, duration of the ignition angle is another important parameter of spark ignition engines. By shortening the ignition duration, the ignition speed increases and the combustion power increases. On the other hand, by shortening the ignition duration too much, combustion is not completed and the combustion power decreases.Therefore, ignition parameters can have a significant impacts on the performance of the entire CCHP system.

The ignition start angle is an operational parameter and can be easily adjusted. However, the duration of the ignition angle can be changed according to the characteristics of the fuel (combustion flame speed), the characteristics of the spark plug and the geometry of the combustion chamber. Fig. 15 shows the effect of ignition parameters on the output power of the CCHP system. It should be noted that the other

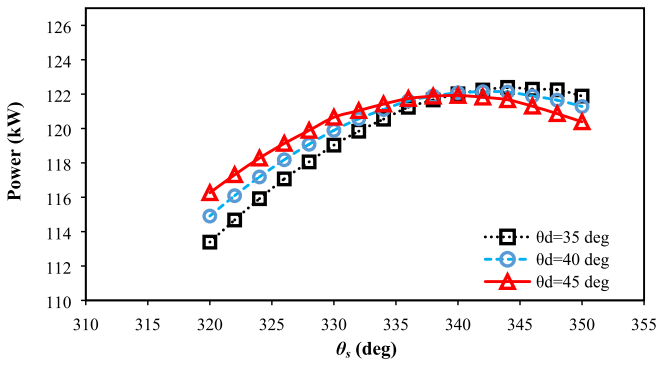

Fig. 15. The effect of spark timing parameters on the output power of the CCHP system.

specifications of the engines are in the default state and the speed of both engines is constant and equal to 3500 rpm. If the duration of the ignition angle is shorter (fast combustion), a significant percentage of the energy from combustion is converted into output power. Thus, if the duration of the ignition angle is 35 degrees and the ignition starts after 344 degrees of engine rotation (16 degrees before the top dead center (TDC)), the maximum power of 122.39 kW can be achieved.

Fig. 16 shows the effect of spark timing parameters on the heating load of the CCHP system. In a specific (fixed) ignition duration, as the combustion time advances, the location of the highest ignition pressure becomes further away from the optimal location of the highest ignition pressure (usually it is located between 2 and 10 degrees after the TDC). Finally, a significant percentage of the energy from the combustion is lost through the engine wall and enters the engine cooling system. In this way, advancing the ignition time causes an increase in heating load. According to the results of Fig. 17, it is clear that the ignition parameters do not have a special effect on the cooling load of the system.

Fig. 18 illustrates the effect of ignition parameters on the overall efficiency of the CCHP system. Because advancing the ignition angle causes an increase in the heating load, it is better to advance the ignition start angle a little to achieve the highest overall efficiency. In this way, the optimal value of the ignition start angle to achieve the maximum overall efficiency of the CCHP system in the ignition start angle and ignition duration is obtained at 336 and 35 degrees, respectively. In these conditions, the maximum value of the overall efficiency of the CCHP system has been reported to be 69.54 %.

In Fig. 19, the influence of ignition parameters on the PES of the CCHP system is presented. Usually, in conditions where the engine has high thermal efficiency, the highest percentage of saving in primary energy consumption for the CCHP system occurs. In this way, at the starting angle of ignition and ignition duration equal to 344 and 35 degrees, the highest PES of 28.26 % is achieved by the proposed CCHP

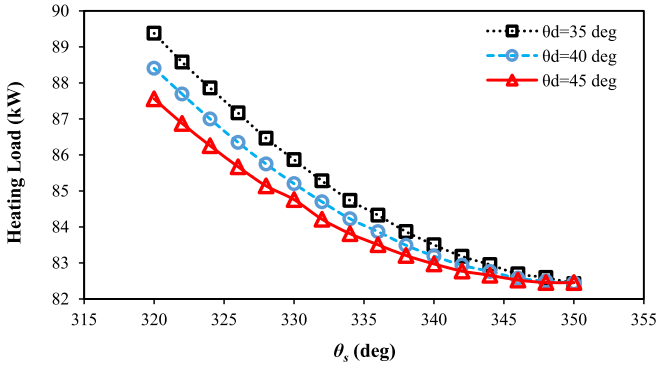

Fig. 16. The effect of spark timing parameters on the heating load of the CCHP system.

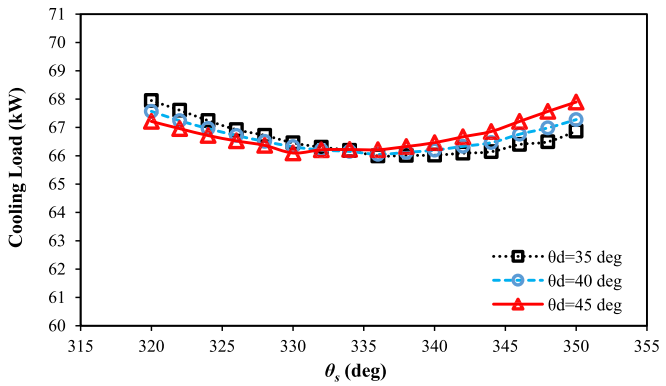

Fig. 17. The effect of spark timing parameters on the cooling load of the CCHP system.

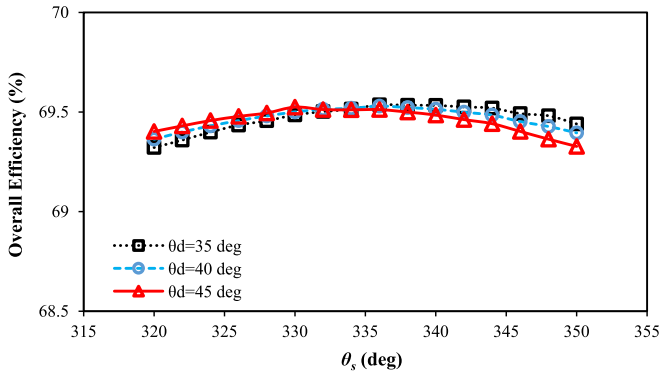

Fig. 18. The effect of ignition parameters on the overall efficiency of the CCHP system.

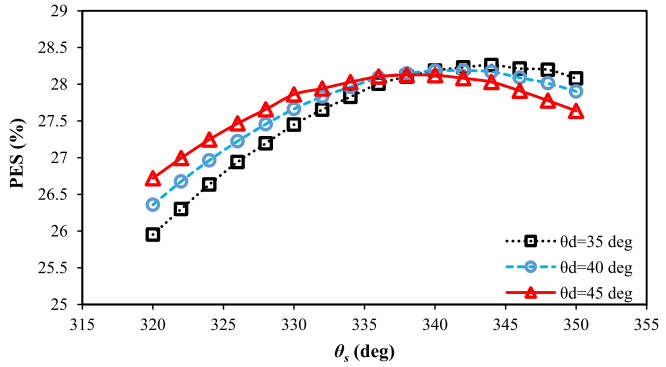

Fig. 19. The effect of ignition parameters on the PES of the CCHP system.

system. Therefore, from the technical perspective, the duration of the ignition angle equal to 35 degrees and the ignition start angle in the range of 336 to 344 degrees are suggested for the proposed CCHP system.

Fig. 20 shows the influence of ignition parameters on annual cost savings (ACS) for the CCHP system. In the condition that the output power is maximum, the maximum amount of annual profit can be achieved. In this way, at the ignition start angle and ignition duration equal to 344 and 35 degrees, more than 41,800 dollars in profit can be achieved per year. This range of ignition parameters is economically more suitable for the system. Also, in Fig. 21, the effect of ignition parameters on the DPP is simulated, by considering different economic inflations and an ignition duration of 35 degrees. It is known that the optimal ignition angle is in the range of 344 degrees, and with the

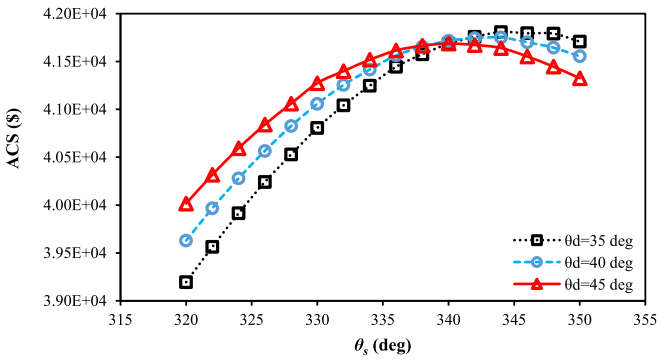

Fig. 20. The effect of the ignition parameters on the ACS of the CCHP system.

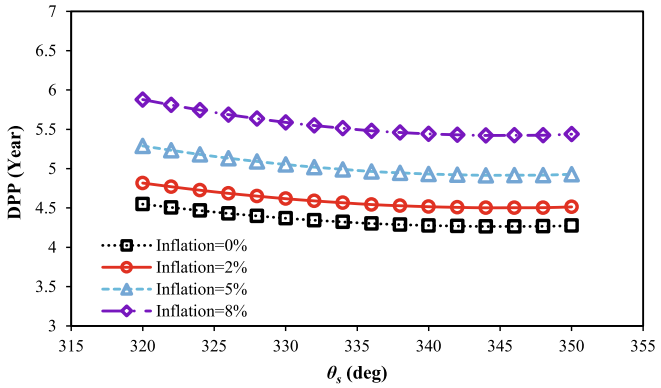

Fig. 21. The effect of the ignition parameters on the DPP of the CCHP system, considering ignition duration of 35 degrees.

increase in economic inflation, the DPP becomes longer.

In Fig. 22, the optimal Pareto front for overall efficiency and simple payback period (SPP) without considering economic inflation as two technical and economic objective functions for the current CCHP system is presented. Also, the most optimal points are collected by Linamp's decision-making method in Table 7.

In the most optimal technical and economic conditions suggested by the Linamp method, the power, heating and cooling loads are equal to 89.4, 48.68 and 41.84 kW, respectively. Also, in these conditions, the overall efficiency, the percentage of PES and the investment payback period without considering inflation and considering 10 % inflation have been calculated as 79.63 %, 39.83 %, 5.75 and 8.97 years, respectively.

Also, other characteristics of the CCHP system in optimal conditions

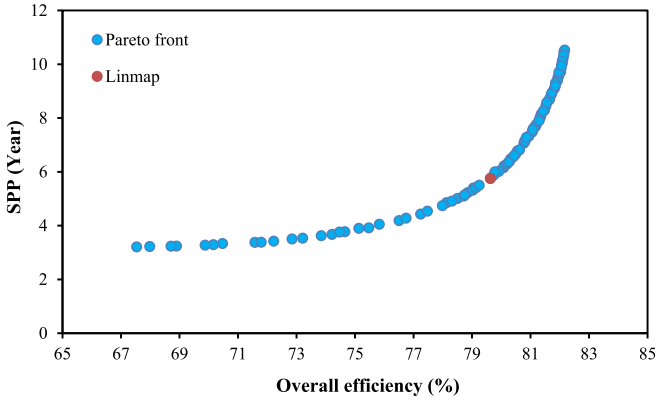

Fig. 22. The optimal Pareto front for the CCHP system for technical and economic objective functions.

in the case of 8 h of work per day are presented in Table 8, and the payback period in optimal conditions is modeled in Fig. 23, taking into account the inflation rate and the number of different operating hours. It is clear that if annual inflation exceeds 10 %, the payback period increases sharply. Also, if the system is used for more hours during the day, the payback period will be shorter (Fig. 23).

6. Conclusions

In this research, with an innovative approach, a CCHP system was modeled numerically with prime movers of the internal combustion engine (ICE) and Stirling engine (SE), and the influence of the technical parameters of these two engines, such as the speeds of the ICE and SE, porosity coefficient and the length of the SE's regenerator, SE phase angle and ICE ignition parameters, on the CCHP technical and economic performances were discussed. In summary, the results of this work are summarized below:

- By using the arrangement of the CCHP system with the hybrid prime movers, due to the suitability of the efficiency of the ICE, at high speed for the SE, the overall efficiency of the CCHP system will reach nearly 64 %, which has increased about 12 % compared to using a CCHP system with only Stirling engine.
- In the SE phase angle range of 87 degrees, because the compression ratio is a suitable value, it is possible to achieve the highest output power of 118.29 kW, the highest amount of savings in annual costs and the shortest payback period. In this conditions, without considering inflation, the SPP is equal to 4.4 years, and considering 8 % inflation, the DPP reaches about 5.63 years.
- The optimal porosity coefficient to achieve the highest values of the overall efficiency and PES for the system is 69 %, and the selection of this range of the porosity coefficient is technically more suitable for the CCHP system.
- Because the maximum amount of output power is obtained in the regenerator length of 20 mm, the shortest payback period of the CCHP system in these conditions is obtained from the length of the regenerator under the same conditions. Thus, the payback period without considering inflation and considering 8 % inflation, has been calculated as 4.11 and 5.19 years, respectively.
- The optimal value of ICE speed to achieve the highest overall efficiency of the CCHP system is about 4000 rpm and the overall efficiency of the CCHP system in this condition reaches nearly 70 %. Also, the PES is maximized in the range of 3700 to 4000 rpm, and this range of ICE speeds can be more suitable from a technical perspective for the CCHP system. If the ICE speed is 3500 rpm, the CCHP system based on the hybrid prime movers has a shorter payback period of about 1.6 years compared to the CCHP system with only the ICE prime mover.
- In a specific (fixed) ignition duration, as the combustion time advances, the location of the highest ignition pressure becomes further away from the optimal location of the highest ignition pressure and finally a significant percentage of the energy from combustion is wasted through the engine wall and enters the cooling system, and heating load increases.
- If annual inflation is more than 10 % and the number of operating hours of the system is less than 6 h per day, the payback period will be more than 15 years, and if annual inflation is less than 5 % and the system operates for an average of about 8 h per day, the payback period will be less than 7 years.

Compared with a natural gas-powered Stirling engine-based CCHP system, the use of CCHP systems based on solar Stirling engines could further reduce carbon dioxide emissions. An efficient, low-cost solar concentrating collector being used to heat the Stirling engine will make this solution attractive. Besides, the use of alternative fuels, including hydrogen as a percentage of internal combustion engine fuel, can help

Table 7
The optimal conditions for the CCHP system using the Linamp decision-making method.

Objective Functions		Decision making variables (design parameters)						
SPP (Year)	Overall efficiency (%)	φ (-)	L_r (mm)	α (deg)	η_r (rpm)	θ_d (deg)	θ_s (deg)	N_r (deg)
5.75	79.63	0.637	35.94	111.27	1352.89	42.23	337.84	3489.19

Table 8
Specifications of the CCHP system in optimal conditions.

Parameter	Value
Power (kW)	89.4
Heating load (kW)	48.68
Cooling load (kW)	41.84
PES (%)	39.83
CO_2ER(Ton)	124.4
CO_2TR ($)	3732.5
ACS ($)	31,019
$PSFC$ $\left(\frac{gr}{kWh}\right)$	203.57
$OSFC$ $\left(\frac{gr}{kWh}\right)$	101.15

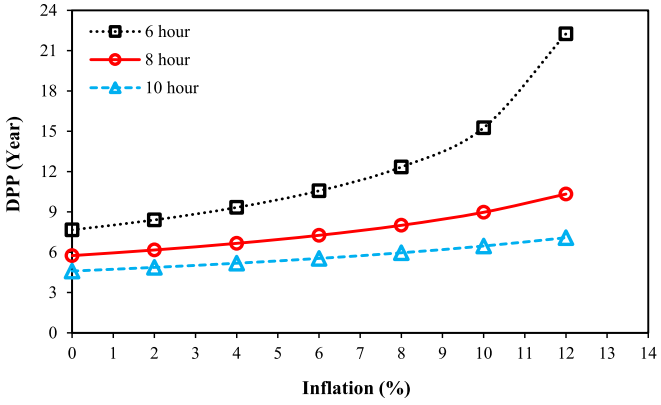

Fig. 23. The effect of annual inflation rate and different number of working hours during the day in optimal conditions.

reduce carbon emissions. Therefore, developing hybrid CCHP systems powered by renewable energy sources (e.g. solar, biomass, hydrogen from renewables), will be the subject of future research.

CRediT authorship contribution statement

Mohammad Sheykhi: Writing – original draft, Visualization, Validation, Software, Methodology, Investigation, Data curation. **Mahmood Mehregan:** Writing – review & editing, Supervision, Project administration, Methodology, Data curation, Conceptualization. **Saeed Ghorbani:** Visualization, Software, Investigation, Data curation. **Amin Emamian:** Visualization, Software, Investigation, Data curation. **Mohammad Hassan Kayhani:** Writing – review & editing, Methodology, Investigation. **Amin Amiri Delouei:** Writing – review & editing, Investigation. **Shahabodin Kharazmi:** Writing – review & editing, Investigation. **Mohammad Kazem Sheykhian:** Writing – review & editing, Investigation. **Shunmin Zhu:** Writing – review & editing, Visualization, Validation, Methodology, Investigation.

Declaration of competing interest

The authors declare that they have no known competing financial interests or personal relationships that could have appeared to influence the work reported in this paper.

Data availability

Data will be made available on request.

References

[1] Ebrahimi M, Keshavarz A. Prime mover selection for a residential micro-CCHP by using two multi-criteria decision-making methods. Energ Build 2012;55:322–31.
[2] Liu M, Shi Y, Fang F. Optimal power flow and PGU capacity of CCHP systems using a matrix modeling approach. Appl Energy 2013;102:794–802.
[3] Chicco G, Mancarella P. Trigeneration primary energy saving evaluation for energy planning and policy development. Energy Policy 2007;35(12):6132–44.
[4] Wang J, Han Z, Guan Z. Hybrid solar-assisted combined cooling, heating, and power systems: a review. Renew Sust Energ Rev 2020;133:110256.
[5] Zarei A, Akhavan S, Rabiee MB, Elahi S. Energy, exergy and economic analysis of a novel solar driven CCHP system powered by organic Rankine cycle and photovoltaic thermal collector. Appl Therm Eng 2021;194:117091.
[6] Al Moussawi H, Fardoun F, Louahlia H. Selection based on differences between cogeneration and trigeneration in various prime mover technologies. Renew Sust Energ Rev 2017;74:491–511.
[7] Meybodi MA, Behnia M. Impact of carbon tax on internal combustion engine size selection in a medium scale CHP system. Appl Energy 2011;88(12):5153–63.
[8] Cho H, Smith AD, Mago P. Combined cooling, heating and power: a review of performance improvement and optimization. Appl Energy 2014;136:168–85.
[9] Shukla A, Vaghasia J, Mistry M. Effect of laser ignition on combustion and performance of internal combustion engine: a review. Energy Conv Manage: X 2022;13:100166.
[10] Szwaja M, Chwist M, Szymanek A, Szwaja S. Pyrolysis oil blended n-butanol as a fuel for power generation by an internal combustion engine. Energy 2022;261:125339.
[11] Puig-Arnavat M, Bruno JC, Coronas A. Modeling of trigeneration configurations based on biomass gasification and comparison of performance. Appl Energy 2014;114:845–56.
[12] Chahartaghi M, Sheykhi M. Energy and exergy analyses of beta-type Stirling engine at different working conditions. Energy Convers Manag 2018;169:279–90.
[13] Rahmati A, Varedi-Koulaei S, Ahmadi M, Ahmadi H. Dynamic synthesis of the alpha-type Stirling engine based on reducing the output velocity fluctuations using metaheuristic algorithms. Energy 2022;238:121686.
[14] Zhu S, et al. A free-piston Stirling generator integrated with a parabolic trough collector for thermal-to-electric conversion of solar energy. Appl Energy 2019;242:1248–58.
[15] Zhu S, et al. Modeling and experimental investigation of a free-piston Stirling engine-based micro-combined heat and power system. Appl Energy 2018;226:522–33.
[16] Erol D, Yaman H, Doğan B. A review development of rhombic drive mechanism used in the Stirling engines. Renew Sust Energ Rev 2017;78:1044–67.
[17] Mehregan M, Sheykhi M, Emamian A, Delpisheh M. Technical and economic modeling and optimization of a ford-Philips engine for power production. Appl Therm Eng 2022;213:118761.
[18] Zhu S, Yu G, Liang K, Dai W, Luo E. A review of Stirling-engine-based combined heat and power technology. Appl Energy 2021;294:116965.
[19] https://energyeducation.ca/encyclopedia/Stirling_engine; 2023. accessed in 4th March 2025.
[20] Ahadi F, Azadi M, Biglari M, Madani SN. Study of coating effects on the performance of Stirling engine by non-ideal adiabatic thermodynamics modeling. Energy Rep 2021;7:3688–702.
[21] Ehyaei M, Ahmadi P, Atabi F, Heibati M, Khorshidvand M. Feasibility study of applying internal combustion engines in residential buildings by exergy, economic and environmental analysis. Energ Build 2012;55:405–13.
[22] Zheng C, Wu J, Zhai X, Yang G, Wang R. Experimental and modeling investigation of an ICE (internal combustion engine) based micro-cogeneration device considering overheat protection controls. Energy 2016;101:447–61.
[23] Wei Y, Du R, Zhang Y, Jamil H, Zhu Z, Liu S. Model investigation of natural gas engine performance to achieve variable heat/electricity ratios for a CCHP system by varying spark ignition timings. Appl Sci 2022;12(15):7544.
[24] Muccillo M, Gimelli A. Experimental development, 1D CFD simulation and energetic analysis of a 15 kw micro-CHP unit based on reciprocating internal combustion engine. Appl Therm Eng 2014;71(2):760–70.
[25] Arbabi P, Abbassi A, Mansoori Z, Seyfi M. Joint numerical-technical analysis and economical evaluation of applying small internal combustion engines in combined heat and power (CHP). Appl Therm Eng 2017;113:694–704.
[26] Balakheli MM, Chahartaghi M, Sheykhi M, Hashemian SM, Rafiee N. Analysis of different arrangements of combined cooling, heating and power systems with internal combustion engine from energy, economic and environmental viewpoints. Energy Convers Manag 2020;203:112253.

[27] Sheykhi M, Chahartaghi M, Pirooz AAS, Flay RG. Investigation of the effects of operating parameters of an internal combustion engine on the performance and fuel consumption of a CCHP system. Energy 2020;211:119041.
[28] Sheykhi M, Mehregan M. Technical and economic modeling of a trigeneration system with EF7 engine as a prime mover. Case Studies Thermal Eng 2023;52:103743.
[29] Kong X, Wang R, Huang X. Energy efficiency and economic feasibility of CCHP driven by Stirling engine. Energy Convers Manag 2004;45(9–10):1433–42.
[30] Karami R, Sayyaadi H. Optimal sizing of Stirling-CCHP systems for residential buildings at diverse climatic conditions. Appl Therm Eng 2015;89:377–93.
[31] Skorek-Osikowska A, Remiorz L, Bartela Ł, Kotowicz J. Potential for the use of micro-cogeneration prosumer systems based on the Stirling engine with an example in the polish market. Energy 2017;133:46–61.
[32] Chahartaghi M, Sheykhi M. Energy, environmental and economic evaluations of a CCHP system driven by Stirling engine with helium and hydrogen as working gases. Energy 2019;174:1251–66.
[33] Sheykhi M, Chahartaghi M, Hashemian SM. Performance evaluation of a combined heat and power system with Stirling engine for residential applications. Iranian J Sci Technol, Trans Mech Eng 2020;44:975–84.
[34] Auñón-Hidalgo JA, Sidrach-de-Cardona M, Auñón-Rodríguez F. Performance and CO2 emissions assessment of a novel combined solar photovoltaic and thermal, with a Stirling engine micro-CHP system for domestic environments. Energy Convers Manag 2021;230:113793.
[35] Sheykhi M, Mehregan M. Comprehensive technical and economic study and optimization of a novel combined cooling heating and power system driven by a four cylinder α type Stirling engine. Appl Therm Eng 2024;236:121869.
[36] Li T, Tang D, Li Z, Du J, Zhou T, Jia Y. Development and test of a Stirling engine driven by waste gases for the micro-CHP system. Appl Therm Eng 2012;33:119–23.
[37] Sheykhi M, Chahartaghi M, Balakheli MM, Hashemian SM, Miri SM, Rafiee N. Performance investigation of a combined heat and power system with internal and external combustion engines. Energy Convers Manag 2019;185:291–303.
[38] Jia J, Paul MC. Thermodynamic and economic evaluation of a CCHP system with biomass gasifier, Stirling engine, internal combustion engine and absorption chiller. Energy Convers Manag 2024;299:117803.
[39] Sanaye S, Chahartaghi M. Thermal modeling and operating tests for the gas engine-driven heat pump systems. Energy 2010;35(1):351–63.
[40] Sheykhi M, Mehregan M, Aliakbari K. A novel differential thermodynamic model for simulating spark ignition engine performance. Energy Convers Manag 2023;298:117794.
[41] Ferguson CR, Kirkpatrick AT. Internal combustion engines: Applied thermosciences. John Wiley & Sons; 2015.
[42] Yeliana Y, Cooney C, Worm J, Michalek D, Naber J. Wiebe function parameter determination for mass fraction burn calculation in an ethanol-gasoline fuelled SI engine. J KONES 2008;15(3):567–74.
[43] Yun KT, Cho H, Luck R, Mago PJ. Modeling of reciprocating internal combustion engines for power generation and heat recovery. Appl Energy 2013;102:327–35.
[44] Sheykhi M, Mehregan M. Improvement of technical performance of heat regenerator of GPU-3 Stirling engine. Energy Rep 2023;9:607–20.
[45] Urieli I, Berchowitz DM. Stirling cycle machine analysis. Bristol: Adam Hilger LTD; 2020.
[46] Alizadeh Kharkeshi B, Mehregan M, Sheykhi M. Sensitivity analysis of energy, exergy, and environmental models for a combined cooling, heating, and power system at different operating conditions of proton exchange membrane fuel cell. Environ Prog Sustain Energy 2023;42(5):e14129.
[47] Chicco G, Mancarella P. Assessment of the greenhouse gas emissions from cogeneration and trigeneration systems. Part I: models and indicators. Energy 2008;33(3):410–7.
[48] Mehregan M, Sheykhi M, Kharkeshi BA, Emamian A, Aliakbari K, Rafiee N. Performance analysis and optimization of combined heat and power system based on PEM fuel cell and β type Stirling engine. Energy Convers Manag 2023;283:116874.
[49] Sanaye S, Chahartaghi M. Thermal—economic modelling and optimization of gas engine-driven heat pump systems. Proc Inst Mech Eng, Part A: J Power Energy 2010;224(4):463–77.
[50] Sheykhi M, Mehregan M, Emamian A, Ghorbani S, Aliakbari K, Delouei AA. Multi-objective optimization of combined cooling, heating, and power (CCHP) system based on CNG engine. Case Studies Thermal Eng 2024;61:105020.
[51] Sheykhi M, Mehregan M, Ghorbani S, Emamian A. Simulating and optimizing the technical specifications of a four-cylinder alpha-type Stirling engine. J Thermal Analy Calorimetry 2025:1–21. https://doi.org/10.1007/s10973-025-14097-9.
[52] Yao Q. Multi-objective optimization design of spur gear based on NSGA-II and decision making. Adv Mech Eng 2019;11(3). https://doi.org/10.1177/1687814018824936. 1687814018824936.
[53] Chahartaghi M, Sheykhi M. Thermal modeling of a trigeneration system based on beta-type Stirling engine for reductions of fuel consumption and pollutant emission. J Clean Prod 2018;205:145–62.
[54] Costea M, Petrescu S, Harman C. The effect of irreversibilities on solar Stirling engine cycle performance. Energy Convers Manag 1999;40(15–16):1723–31.
[55] Formosa F, Despesse G. Analytical model for Stirling cycle machine design. Energy Convers Manag 2010;51(10):1855–63.
[56] Ahmadi MH, Ahmadi MA, Pourfayaz F, Bidi M, Hosseinzade H, Feidt M. Optimization of powered Stirling heat engine with finite speed thermodynamics. Energy Convers Manag 2016;108:96–105.
[57] Timoumi Y, Tlili I, Nasrallah SB. Design and performance optimization of GPU-3 Stirling engines. Energy 2008;33(7):1100–14.
[58] Ni M, et al. Improved simple analytical model and experimental study of a 100 W β-type Stirling engine. Appl Energy 2016;169:768–87.
[59] Ahmed F, Zhu S, Yu G, Luo E. A potent numerical model coupled with multi-objective NSGA-II algorithm for the optimal design of Stirling engine. Energy 2022;247:123468.
[60] Toghyani S, Kasaeian A, Hashemabadi SH, Salimi M. Multi-objective optimization of GPU3 Stirling engine using third order analysis. Energy Convers Manag 2014;87:521–9.
[61] Bataineh KM. Numerical thermodynamic model of alpha-type Stirling engine. Case Studies Thermal Eng 2018;12:104–16.
[62] Hosseinzade H, Sayyaadi H. CAFS: The Combined Adiabatic–Finite Speed thermal model for simulation and optimization of Stirling engines. Energy Convers Manag 2015;91:32–53.
[63] El-Ghafour S, Mikhael N, El-Ghandour M. Energy and exergy analyses of Stirling engine using CFD approach. J Adv Res Fluid Mech Thermal Sci 2021;77(1):100–23.
[64] Kopeliovich D. Bearings in internal combustion engines. ed: SubsTech: http://www. substech. com/dokuwiki/doku. php. 2012.
[65] Kakaee A, Karimi M. A comparative study on influence of natural gas composition on the performance of a CNG engine. Mapta J Mech Indus Eng (MJMIE) 2018;2(3):9–18.
[66] Barjaneh A, Sayyaadi H. A new closed-form thermodynamic model for thermal simulation of spark ignition internal combustion engines. Energy Convers Manag 2015;105:607–16.
[67] Daoud JM, Friedrich D. Design of the multi-cylinder Stirling engine arrangement with self-start capability and reduced vibrations. Appl Therm Eng 2019;151:134–45.
[68] Berchowitz DM, Kwon Y-R. Multiple-cylinder, free-piston, alpha configured Stirling engines and heat pumps with stepped pistons. Google patents. 2007.
[69] Berchowitz DM. Double acting Stirling engine phase control. Google patents. 1983.